Recent Trends in Fibrous Material Science

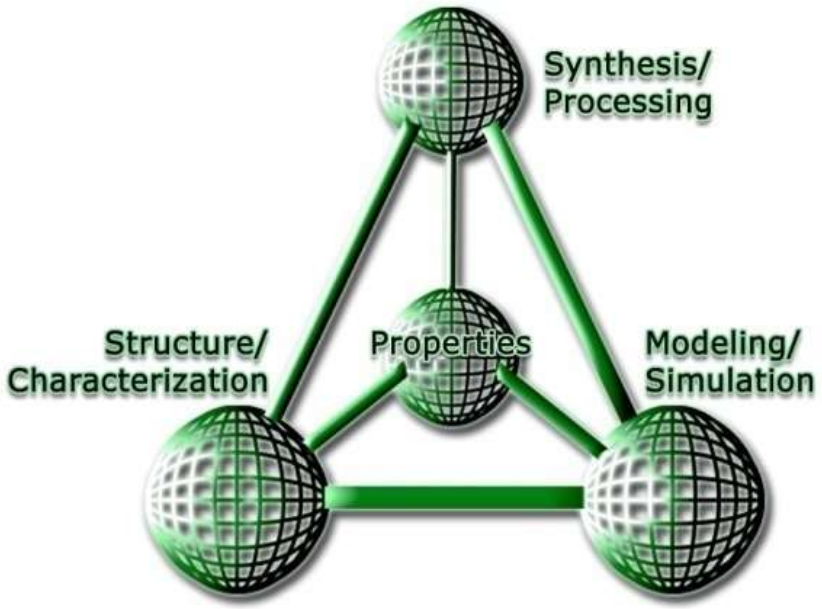

Volume - V
September - 2019

Key Authors and Editors

Rajesh Mishra
Jiri Militky

TECHNICKÁ UNIVERZITA V LIBERCI
Fakulta textilní

TECHNICAL UNIVERSITY OF LIBEREC
Faculty of Textile Engineering

TECHNICKÁ UNIVERZITA V LIBERCI
Textilní fakulta Katedra materiálového inženýrství

Doc. Rajesh Mishra, B.Tech., PhD
Prof. Ing. Jiří Militký, CSc. EURING

RECENT TRENDS IN FIBROUS MATERIAL SCIENCE

Liberec 2019

Chapter 1

Characterization and Strength Distribution of Fibrous Glass Tapes

Jiří Militký[1], Mohanapriya Venkataraman[1], Vijay Baheti[1], Jana Novotná[1], Roman Pulíček[1], Alžbeta Samková[1], Karolína Voleská[2], Pavel Srb[3], Dana Křemenáková[1], Rajesh Mishra[1] and Bijoya Kumar Behera[4]

[1]Technical University of Liberec, Faculty of Textile Engineering, Department of Material Engineering, Liberec 46117, Czech Republic.
[2]Technical University of Liberec, Department of the Preparation and Analysis of Nanostructures, CxI, Czech Republic.
[3]Technical University of Liberec, Faculty of Mechanical Engineering, Department of the Design of Machine Elements and Mechanisms, Czech Republic.
[4]Department of Textile Technology, Indian Institute of Technology Delhi, India.

1. INTRODUCTION

Composites have a plenty of advantages in comparison with classical construction materials. Major benefit is low weight, tunable corrosion resistance, high fatigue strength, and simples assembling. They are combinations of different materials, where the individual separate constituents are giving to them the required mechanical strength or stiffness or functional properties. Composites are at least composed of matrix phase and dispersed phase. Typically, they have bulk properties significantly different from those of any of the components.

Matrix phase with continuous character has following roles:

- Keep the fibers together and enhances a transfer of the loads,
- improves stiffness and shape stability,
- isolate the reinforcement - each fiber can act independently in presence of a delamination or a crack,
- defines the surface properties,
- protects the reinforcement from chemical attacks and mechanical damages.

Matrix is usually a more ductile and less hard phase. It holds the dispersed reinforcement phase.

Reinforcing phase with discontinuous character embedded in the matrix is responsible for definition the structural order and geometry of composite and for load bearing. In a fibrous composite between 70 and 90% of the loads is carried by this phase. This phase has major contribution for functional properties. Provide strength, stiffness, thermal stability and majority of the other properties of the composite.

Benefit of composites is mainly due to their small density ρ combined with higher initial modulus E enabling to create lighter structures with the required performance.

It is clearly demonstrated on the example of relation between mass m of beam (length l and cross section S) with modulus E axially elastically deformed to small dl under load P. From definition of initial modulus it can be calculated weight of beam as $m = P\,l^2\,\rho/(\mathrm{d}l\,\mathrm{E})$. The same deformation under given load can be obtained for smaller mass of beam if it will be possible to reduce density and improve modulus of beam material.

The major advantages of composites in comparison with traditional metals are:

Lightness. Density ρ of composites is very low in comparison with metal and initial modulus of reinforcement E is near to metals. It is then possible to manufacture composites with mechanical properties similar to the metals (in terms of strength and stiffness) but with a very low weight.

Fatigue. Composites have high levels of fatigue strength. Traditional metals such as steel exhibit a level of fatigue strength around 50% of their static strength, while for composites this percentage reaches more than 90%.

Corrosion resistance. Corrosion happens in traditional metals when they interact with water or air. For majority of applications is then necessary to use the special coatings that can negatively affect other mechanical properties. The external surface of a composite is generally polymeric and the resistance to chemical attacks is very high.

Shape stability. Since the volumetric thermal expansion coefficient of composite material is much lower than metals, they have higher levels of dimensional stability. Composite are able to retain their shapes when exposed to thermal gradients, variations of pressure and moisture modifications

Multi-functionality. The control on all the components that form composites, allow adding different fillers capable to modify mechanical, thermal, electrical and other properties by simple way.

Glass fibers (GF) are commonly used as reinforcement phase in composites due to their no flammability, strength, abrasion resistance, cost effective processing and reasonable price in production. Epoxy resin (EP) is an excellent thermosetting resin. It has superior mechanical properties, electrical insulation, chemical resistance, heat resistance and adhesion properties compared to currently used unsaturated polyester resins. It is well known that EP is used in nanocomposites (fine powder reinforced materials) for insulating, protective and load bearing structures.

EP/GF composites are a mature and widely industrially used composite material. They have low weight, high strength, large modulus, good corrosion resistance, excellent electrical properties, and wide source of raw materials, good process ability and high production efficiency. Their functions have become important materials for defense structures and advanced products as bulletproof helmets, bulletproof barriers, helicopter wings, containers, civil aircraft bars, sporting goods, various types of high temperature resistant products, and recently reported tire cords with excellent performance.

Glass based fabrics and tapes have generally high strength along with a relatively low density, high thermal resistance, good insulate characteristics, resistance to microorganisms, as well as good chemical resistance to oils, fats and organic solvents,

acids and alkalis in the pH-range from 3 to 9. These properties can be leveraged while using in end-use applications. Some of the disadvantages are sensitivity to strong alkalis, surface corrosion, fragility and relatively hard process ability [7 - 13].
For effective applications of glass fiber reinforced epoxy composites and hybrid tapes the information about their properties is very important. This chapter deals with the preparation, characterization of geometrical properties and evaluation of strength distribution of stabilized hybrid composite tapes, tows and glass fibers. The comparison of epoxy resin glass fibers tapes with glass fiber reinforced polypropylene tapes is also accomplished.

2. SELECTED MATERIALS

The production and development of high-performance glass fiber comes from the high-end application requirements of composite materials and the mature and innovative development of glass fiber technology, which enables the design ability of glass fiber and its excellent comprehensive performance. Typical glass fibers properties from China producer are summarized in the tab. 1.

Table 1. Typical properties of glass fibers presented by Hengshi Co. China.

Property	**standard**	**unit**	**value**
density	ASTM D1505	kg m^{-3}	2580
Thermal expansion	ASTM C338	K^{-1}	5,51 10^{-6}
Softening temperature	ASTM C338	^{o}C	921
Initial modulus	Acoustic	GPa	89

Typical glass tow properties from Slovakia supplier are summarized in the tab. 2.

Table 2. Typical properties of glass tow StarRov 086 1200 presented by Johns Maneville Co. (Slovakia supplier)

Property	**unit**	**value**
Fineness	tex	1200
Filament diameter	μm	16
Tensile strength	N	450

Selected properties of hybrid tape (composite glass tow fused with polypropylene fibers) COMPOFIL presented by Hengshi Co., China are summarized in the tab. 3.

Table 3. Mechanical properties of COMPOFIL glass/PP (Hengshi, China)

Property	**unit**	**Mean value**
Glass fiber content	%	60
Tensile strength	MPa	620
Tensile modulus	GPa	33
Bending strength	MPa	390
Bending modulus	GPa	25

One of aim of this work is comparison of some advanced form of tows (rectangular cross section) from Slovakia branch of producer Johns Maneville Co. and tow from glass fiber ER-12-988, Zhejiang Tongxiang Jushi Group Co. Ltd. with hybrid tapes prepared by spreading technology (on the pilot line described in section 4.3) and with hybrid tape (linear composite) COMPOFIL prepared by fusion of glass tow and polypropylene fibers. Materials are specified in tab. 4.

Table 4 Specification of selected materials

Material	**Glass filament**	**Resin**	**Producer**	**abbreviation**
Tow	ASTM D1505	no	Slovak	**SL**
Tow	ER-12-988	no	China	**CH**
Hybrid tape	ASTM C338	CHS-EPOXY 200 V 55	Czech-pilot	**SLT**
Hybrid tape	ER-12-988	Polypropylene	China	**CHT**

For the preparation of hybrid tapes SLT (see. fig. 1d) the glass tows StarRow 1200 (SL) from Slovak supplier were used (see. fig. 1b). The glass filaments are made form alumino-borosilicate E- glass in accordance with ASTM D 578.

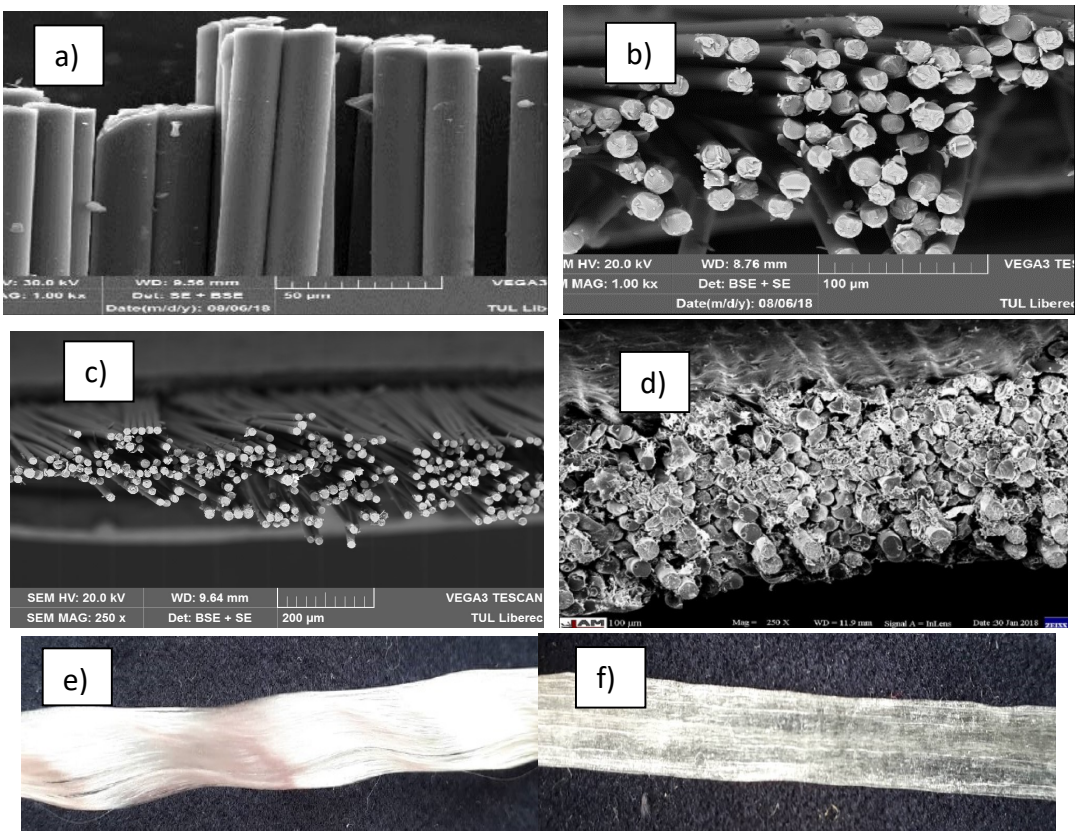

Fig. 1 Material SL and SLT (a) glass fibers in tow-broken surfaces, (b) and (c) glass fibers in tow –cross-section, (d) glass fiber in tape (e) tow longitudinal view, (f) tape longitudinal view

The mechanically spread tows SLT (see chap. 4.3) were coated with epoxy resin dispersion CHS-EPOXY 200 V 55 with catalyst and pre cured at 80°C for 24 hours.
From fig. 1 it is visible that tows and tapes are with rectangular cross section and individual fibers are relatively even. Tow is slightly curly and tapes are straight.
For comparative purposes, the glass tows CH form China producer were selected (see fig. 2).

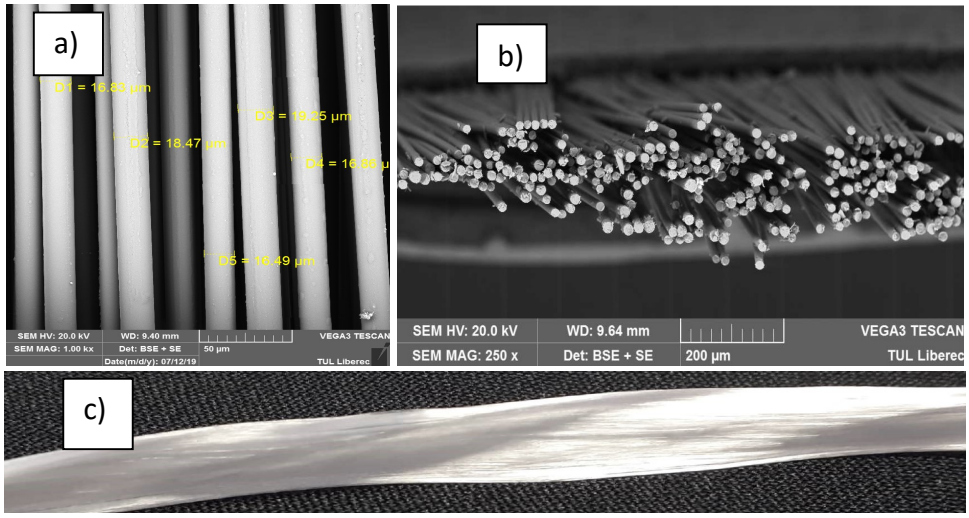

Fig. 2 Material CH (a) glass fibers in longitudinal view, (b) glass fibers in tow – cross-section, (c) tow longitudinal view

From fig. 2 it is visible that tows are with rectangular cross section and are slightly curly.
Geometry of hybrid tape COMPOFIL with polypropylene thermoplastic (material CHT) is shown in fig. 3).

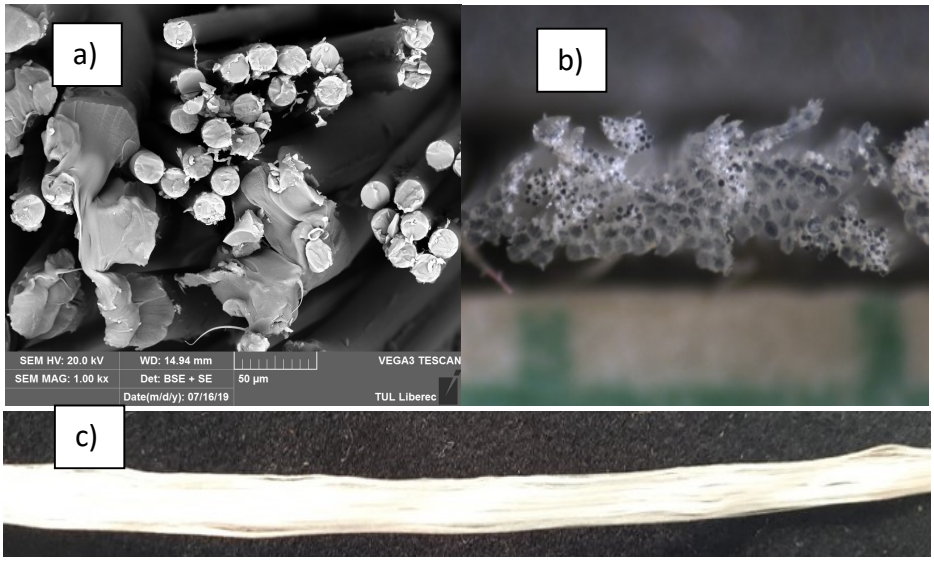

Fig. 3 Material CHT (a) glass fibers/pp fibers in longitudinal view, (b) tape cross-section, (c) tow longitudinal view

Tapes CHT are as well slightly non parallel with relatively flat rectangular cross section and are not so regularly arranged as tapes SLT because during their production is not used standard spreading. The individual filaments in materials CH and SL were obtained by direct separation from tows.

3. COMPOSITE MATERIALS WITH GLASS REINFORCEMENTS

Nowadays, the composite engineers are focusing on the development of new stronger, tougher, lightweight structural materials supporting latest technologies and design concepts for the complex shaped structures like aircraft, automotive structures and large wind turbine blade structures. The development of composite materials improves their performance based on the reinforcement of one, two or more fibers in a single polymeric matrix, which leads to the advanced material system called hybrid composites with a great diversity of material properties. This is a major challenge that can only be met through an understanding of the relationships between materials architecture and mechanical response. The positive or negative hybrid effect of selected mechanical property from the rule of mixture behavior of carbon/carbon/ epoxy and glass/carbon composites were studied.

Glass fiber is the most widely used inorganic non-metallic material in composite reinforced substrates. With the continuous development of high-performance and multi-functional materials, advanced manufacturing technology, low cost and application expansion, higher requirements are placed on the cost performance of glass fiber reinforced substrates. In recent years, different grades of high performance glass fiber have been produced. The promotion and application of composite materials in new energy, transportation, construction, chemical and other fields is changing production of glass fiber “from the big to the strong”.

3.1 Glass Fiber / Epoxy Resin Composite

Glass-fiber reinforced polymer matrix composites have extensively been used in various fields such as aerospace industries, automobiles, marine, and defense industries because of their high specific strength and stiffness. Their main advantages are good corrosion resistance, lightweight, dielectric characteristic, and better damping characteristics than metals. But these composite materials are easy to suffer low energy impact during service, and also more sensitive to impact load. When the velocity is high, the composite laminates will be broken down; while the impact velocity is low, the damage will generate different forms, such as matrix cracking, fiber breakage and delamination [7, 8]. At low-impact velocities the behavior of the composite is primarily dictated by the viscous behavior of the epoxy resin. The role of the microstructure becomes more noticeable at higher impact velocities. The damage of most composite materials is not caused by a single impact, but often after several low-energy impacts. When the composite material is subjected to low-energy impact, most of the cases have no obvious visual damage, but it will cause invisible shallow surface delamination on the laminated surface, thus forming a potential danger [8,

14]. The existence of internal damage can cause the composite material to great loss in strength and stiffness.

Epoxy resin as matrix are widely used in the production of glass-fiber composites due to their wetting power and adhesion to glass fiber, low setting shrinkage, considerable cohesion strength, adequate dielectric characteristics, and thermal properties. However, the application of epoxy resin and epoxy resin–matrix composites is usually limited owing to the relatively poor thermal stabilities and wear-resistance. In order to enhance the wear resistance and thermal stabilities, many studies have been carried out. One of these is the modification of matrix. Many hard particulate types of filler made of ceramic or metal particles have been tried to modify the epoxy resin–matrix composites for that purpose by several researchers [15- 19]. Their results show that the addition of various ceramic particles into epoxy matrix enhances the friction and wear characteristics of the composites. The use of such hard particles increases the dry sliding friction coefficient and abrades the counter face [4, 5].

Glass reinforced epoxy composites filled with various compositions (1, 3, 5 and 7%) of cloisite clay particles were prepared by Jeyakumar [24]. The as-prepared samples of unfilled or neat epoxy glass fiber composites and clay particles reinforced composites were tested for their morphological and mechanical properties. The morphological behavior was investigated by the use of scanning electron microscope for visualizing the distribution of nanoclay in the epoxy matrix. The homogeneity dispersion of the nanoclay was confirmed from the high resolution scanning electron microscope (HR-SEM) analysis. The study on mechanical properties such as tensile, flexural and impact test was carried out test the hardness of the prepared reinforced composites. The mechanical studies were carried out for all the compositions of 1, 3, 5 and 7% of the epoxy matrix composites. For 5% reinforced clay composites, the tensile strength and modulus were found to increase by 23.58 and 23.66% when compared to the unfilled composite. Further increase in nanoclay content decreases the tensile properties of nanocomposite. For the flexural strength and modulus for 5% nanoclay reinforcement, there is an increase of 34.10 and 53.86%, respectively, when compared to the unfilled composite. The impact strength for 5% reinforcement of nanoclay has an increase of about 29.65%, whereas for all the other compositions it showed a decreasing trend. The results of micro hardness, interlaminar sheet strength (ILSS) and compressive strength were discussed in detail for all the compositions [24].

3.2 Glass Fiber / Polypropylene Composite

Glass fiber reinforced polypropylene refers to a modification method in which polypropylene is used as a matrix and glass fiber is a reinforcing phase, which is compounded by a suitable processing method to improve the physical properties of polypropylene. Glass fiber reinforced polypropylene composites have the advantages of light weight, high strength, corrosion resistance, etc. Compared with polypropylene, their mechanical properties can be increased by two to three times,

like rigidity and resistance. Other properties such as creep can be increased by a factor of two to five times, and the heat distortion temperature is also greatly improved.
In the 1950s, American companies produced short-fiber reinforced polypropylene and realized industrial production. In the 1970s, medium-long fiber reinforced polypropylene materials appeared. In recent years, research hotspots have focused on continuous long-fiber reinforced polypropylene.
Barkoula [25] described the fatigue behavior of newly developed all-polypropylene (all-PP) tapes and composites, with reference to the composite processing conditions and compared this behavior with commercial alternatives. All-PP tapes are highly oriented and their failure behavior follows that of other highly oriented polymers. All-PP woven composites fail ultimately due to PP tape failure. However, this failure mode is preluded by delamination of fabrics in the woven structure. Consolidation pressure plays a decisive role in controlling the interlaminar properties and hence controls the delamination resistance and furthermore the fatigue limit of the composite. Comparison of all-PP woven composites with commercial alternatives based on glass and natural fibers reveals the excellent relative performance of all-PP composites under fatigue loads. Fatigue properties of all-PP composites are however sensitive to the testing temperature and elevated temperatures can lead to a rapid reduction of the fatigue resistance of these all-polymer systems [25].
The creation of highly oriented, co-extruded polypropylene (PP) tapes allows the production of recyclable “all-polypropylene” (all-PP) composites, with a large temperature processing window and a high volume fraction of highly oriented PP (>90%). The wholly thermoplastic nature of these ‘self-reinforced’ composites implies that the mechanical performance may vary with temperature. The mechanical performance of all-PP composites by measuring the mechanical properties of highly oriented PP tapes and subsequent all-PP composites at a range of temperatures by static and dynamic testing methods in described in [26]. The time–temperature equivalence of all-PP composites is investigated by creating master curves of dynamic modulus and tensile strength. A comparison of the performance of these composites with commercial glass fiber reinforced polypropylene composites is included [26].
There are many factors affecting the performance of glass fiber reinforced polypropylene materials, such as glass fiber content, glass fiber length and so on. The modulus of glass fiber reinforced polypropylene was found to be proportional to the glass fiber content [27]. By reducing the diameter of the glass fiber, the strength of the short glass fiber reinforced polypropylene system can be improved, but it is still not as strong as that of the long glass fibers [29]. Thomason [28] studied the reinforcing materials with high glass fiber content, and found that there is an optimal range of fiber content in the reinforcing materials, which is 40% to 50%.

3.3 Application of Glass Reinforced Composites

Wind Turbine
A wind turbine is a turbine that uses wind energy to power it (see fig. 4).

Fig. 4 Wind Turbine

Wind turbines are like the air intakes of jet engines. When air enters, it first encounters a fixed set of blades, called the stator, which directs air into a set of rotatable blades called the rotor. The air pushes the rotor and appears on the other side, at which point the air flows at a slower rate than it flows outside the turbine. The shield is shaped such that it directs relatively fast flowing air outside into the area behind the rotor.

The fast flowing air accelerates the slowly moving air, causing the area behind the turbine blades to become low pressure to absorb more air through them.

The strength and stiffness of the wind turbine blade material is the key to determining the performance of the wind turbine. At present, the materials used in wind turbine blades have been developed from wood, canvas, etc. to metal (aluminum alloy), glass fiber reinforced composite (glass reinforced plastic), carbon fiber reinforced composite materials, etc. Among them, the new fiberglass blade material is light in weight and high in specific strength.

The design is strong, the price is relatively cheap and other factors, and it has become the mainstream of large and medium-sized wind turbine blade materials.

However, with the development of wind turbine blades towards ultra-large size and light weight, composites have also reached the limit of their performance. Carbon fiber composites are gradually applied to ultra-large wind turbine blades [30].

In order to meet the requirements of the use of wind turbine blades, glass fiber is also undergoing technological innovation. For example, Windstrand new generation of reinforced glass fibers developed by Owens Corning can improve blade performance without increasing blade costs. According to reports, WindStrand (Product info: tensile modulus in unidirectional composite with 55 % of glass filaments is 51,2 GPa and strength is 1,15 GPa) can improve the hardness and strength of the blade, so that the blade has good fatigue resistance, which can improve the wind resistance of the blade, increase the life of the blade, and increase the energy conversion rate of the blade. Compared to conventional E-glass, the enhanced WindStrand reduces the weight of the blade by 10%, which ultimately reduces the cost of wind power.

Automotive interior

Glass fiber reinforced polypropylene and polyamides for example are superior construction materials for automotive sector having an outstanding performance.

Applications like frontends, dashboard carriers, door modules and underbody structures based on these materials currently dominate this market segment (see. fig. 5).

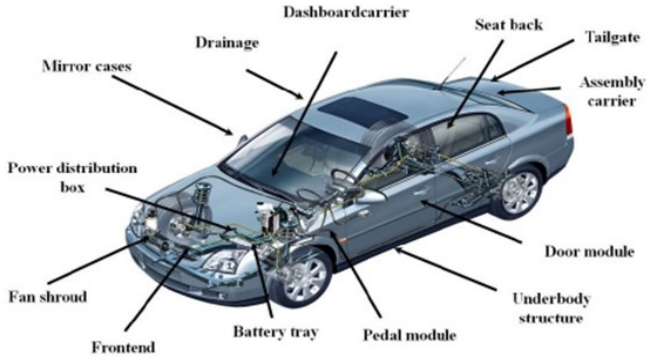

Fig. 5 Application examples of glass reinforced composites in automotive

4. CONTINUOUS FIBER REINFORCED COMPOSITES

The starting material for composites are multifilaments (wires), i.e., the strands (rovings) that are formed by a combination of filaments (filaments) of low fineness (diameter below 20 μm) required to ensure low bending stiffness. The number of cross-sectional filaments (continuous fibers) ranges from 1k to 24k (number of filaments in roving in thousands). Twisted multifilaments, i.e. yarns, have an approximately circular cross-section and the density of the arrangement increases with increasing twist. However, the twist decreases the initial modulus and yarn strength. Also, penetration of the resin or its components is not easy. Rovings (tow) are with slight (protective) twist (less than 50 turns / m) and are suitable for the manufacture of prepregs. They usually have an oval cross section and their porosity decreases toward the center of the body. Spread tow tape (tape) is characterized by the fact that their width is multiplied by more than 3 times the diameter of the original multifilament. The individual filaments are here much more closely arranged and behave like a bunch of identical long parallel threads with constant porosity in cross section. This leads to a better utilization of the strength of individual filaments and to a reduction in the thickness (by 20 to 30%) [3-6]. The problem is to ensure cohesion and then resin saturation. The resin must ensure the storage life of the tapes. To improve mechanical properties of resins, it is preferred to use suitable fillers (particulate systems). The resulting stabilized hybrid composite tapes comprising an optimally arranged resin-bonded fibrous phase and surface nanoparticles with functional particles will allow the production of composites in particular by the technique of precision robotic winding [22].

4.1 Forms of Fiber Reinforcements

Continuous fiber reinforcements are available in the form of tows or tapes (unidirectional - *ud*) composed from continuous (multi)filaments as starting materials for creation non-crimp, woven, braided and wounded fabrics. The tows are not

parallel because the individual filaments can be crimped or locally not disoriented. Their limitations are due to splitting, wrinkling and folding during manufacturing and handling as well. The spreading tows into tapes are changing arrangements of fibrous phase to the direction parallel with machine axis (see fig. 3).

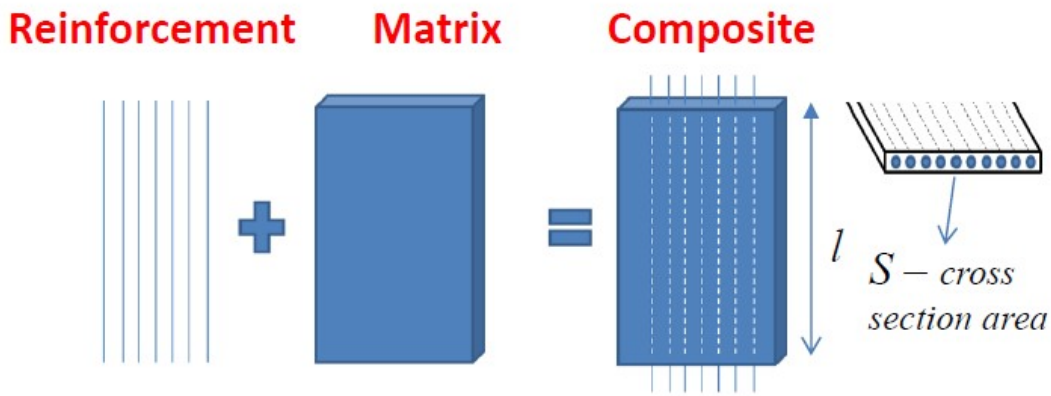

Fig. 6 Typical unidirectional composite

Multifilament yarns are typically used for the production of glass reinforced composites, where filaments are glued together to ensure compactness and improved properties (strength, evenness) [1, 2]. The starting material for glass fibers based composites is multifilaments (tow), i.e., the strand that is formed by a combination of filaments (filaments) of low fineness (diameter below 20 μm) required to ensure low bending stiffness. The number of cross-sectional fibers ranges from 1k to 24k (number of filaments in roving in thousands). Twisted tows, i.e. yarns, have an approximately circular cross-section and the packing density increases with increasing twist. However, the twist negatively affects the initial modulus and yarn strength. In addition, penetration of the resin or its components is not so easy. Tows (rovings) are usually straight or with slight (protective) twist (less than 50 turns/m) only and are suitable for the manufacture of prepregs. They usually have an oval cross section and their porosity decreases toward the center of the body. The roving is temporarily form stabilized by surface spin finishing. Suitable for epoxy matrices are spin finish as mixture of acrylate polymers and epoxy/silane. Some companies produce glass roving with starch sizing which are unsuitable for epoxy mats. For industrial glass roving, the major problem is due to very high speeds in the production itself and the subsequent spinning of the cross-winding fibers, uneven disconnection of the individual fibers occurs. If composite material from such a roving is prepared, optimal mechanical properties cannot be achieved. It is due to the reason that when the composite is loaded, only the percentage of fibers can be loads bearing.

Tapes (spread tow) are characterized by the fact that there are parallel (without bends and twists) and their width is much higher than thickness or the diameter of the original multifilament (see fig. 7).

The individual filaments in tapes behave like a bunch of identical very closely arranged parallel threads. This leads to a better strength bearing by individual filaments and to a reduction in the thickness (by 20 to 30%) and hence the areal

density of the composites [3-6]. The challenge is to ensure cohesion and form stability by using of pre-cured resin with sufficient through-resin saturation. The resin must ensure the storage life of the tapes and subsequent compatibility with resin used for composite preparation. To improve mechanical properties of resins, it is beneficial to fill resin phase with suitable particulate fillers (nano-composites).
The final hybrid composite tapes with parallel-arranged resin-bonded fibrous phase embedded in resin matrix (unidirectional composite – UD) and filled by nanoparticles with functional properties allow to production of special 2D or 3D fabrics or composites especially by precision robotic winding.

4.2 Spread-tow technology

Spread-tow technology is one of simplest method for achieving ultra-lightweight composite material [3]. Carbon based spread-tow materials were developed by Oxeon AB (Sweden; www.oxeon.se). Sakaiovex (Japan; www.sakiovex.co.jp) is developing similar products, and relatively recently Formax (UK; www.formax.co.uk) and G. Angeloni (Italy; www.g-angeloni.com) [20].
Spreading leads to geometric rearrangement of fibrous tow into a thinner, flatter and more oriented tape (see fig. 7).

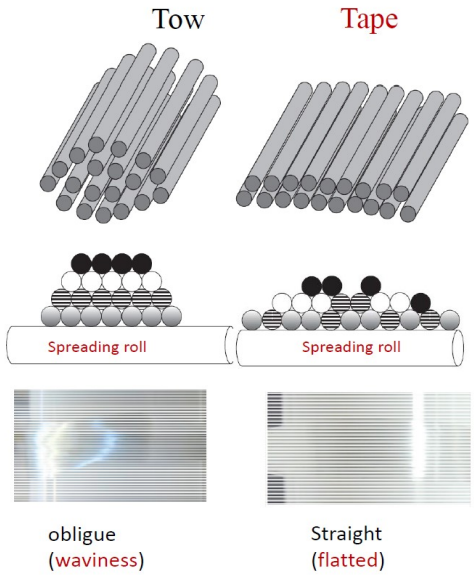

Fig. 7 Spreading tow into tape (partially adopted from [20])

This unidirectional tape can then be used to produce thin woven fabrics or braided (wounded structures).
It is possible to spread carbon, glass, aramid and polymer fibers. Spread-tow reinforcements can weight as little as 15 g/m^2 with a thickness of only 0.02 mm. Spreading enables the tailoring of *thickness, flattenes, width, areal mass* as well as other properties, such as *resistance to crack propagation* for improved damage

tolerance. The flatness of tape results in more efficient load-carrying capability. The spreading technology is schematically shown in fig. 8.

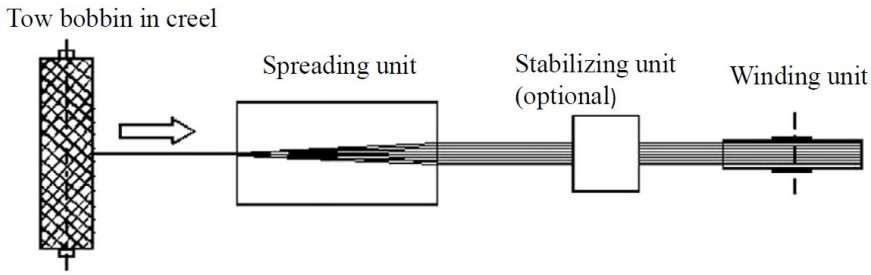

Fig. 8 Typical spreading technology [6]

Generally, the active and passive methods have been proposed to spread a tow into tape. The **active spreading** uses energy to spread the roving. The use of an airflow (pressure or suction) in a small gap or the transfer of (ultra-) sonic waves and vibrations into the filaments are typical examples (see fig. 9).
Passive spreading uses only mechanical tension. A constant movement over different geometries like spreading bars, convex or other geometrical guiding elements are typical examples (see fig. 9).

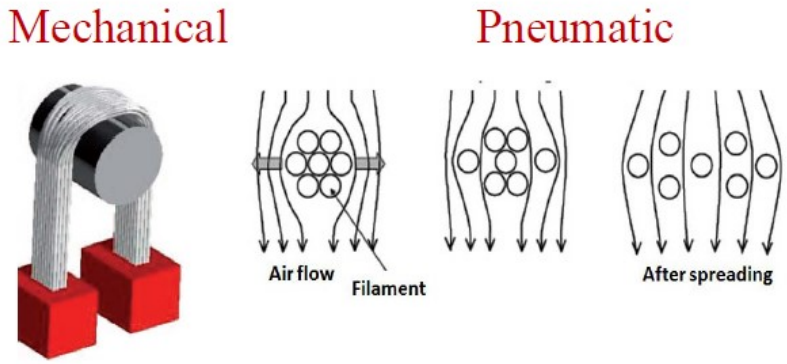

Fig. 9 Passive (mechanical) and active (pneumatic) tow spreading.

One of most advanced technology for continuous and stable spreading of tows is based on sucking of air. The air duct is located between guide rolls. As the air flows through the air duct with the help of the vacuum, the tow sags downward toward the air flow direction because the tow tension is controlled to become low [6]).
For preparation of hybrid tapes containing the prototype line was created (see fig. 10) by company Večerník s.r.o. The pilot plant is a model which however fulfilled the purpose of producing reproducible tapes made of glass roving and special epoxy resin. Special drive unit for to automatic control the speed of initial unwinding of roving and final winding under constant strain of finished tape was developed as well.

Fig. 10 Prototype line for production of hybrid tapes

In the first part of prototype line roving passes through the smooth steel rod system. In this part, the effort is to mechanically separate the individual fibers and pull on the roving to ensure a constant disconnection of the individual fibers. It would be possible to achieve a homogenous shutdown of the individual fibers to ensure their perfectly parallel arrangement which would at least ensure the approximation of the theoretical value of the glass fiber strength. Tape form stability before making composites is realized by using of epoxy matrix. In order to ensure sufficient epoxy matrix content, three epoxy dispersion-based coating stations are used in the prototype line and at each of the stations the impregnated roving is dried at elevated temperatures. In terms of sifting the fibrous structure, the first deposit is most important, further deposits are mainly due to the fact that the layers are interconnected with each other in the formation of the composite. After the last coating of the epoxy dispersion with the catalyst, a cross-winding is performed on a roll. The general view and SEM image of final hybrid tapes is shown in shown in fig 11.

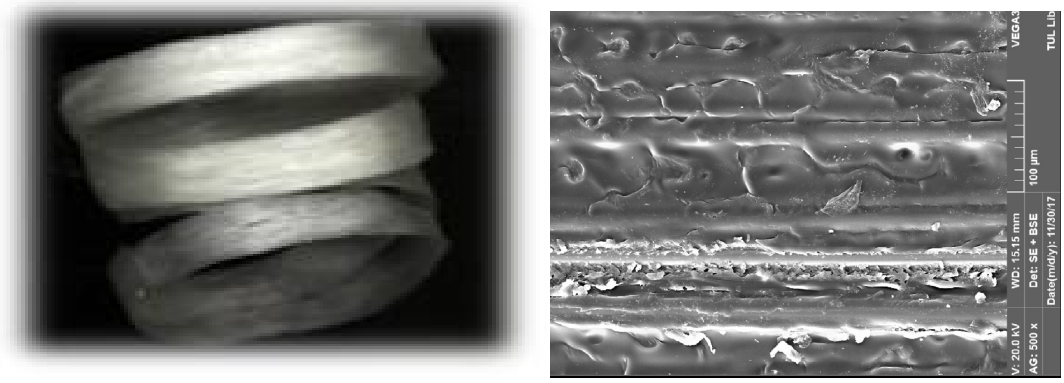

a) b)

Fig. 11 Hybrid tape a) general view, b) SEM image with abraded center for allowing visibility of glass fiber.

The hybrid tapes prepared on the prototype line with adding of fly ash fillers (original, dry milled, wet milled see. fig. 12) into epoxy matrix were comprehensively tested [23]. It was found that hybrid tapes containing 1% by weight of wet milled fly ash

particles exhibited the greatest improvement in bending properties (the bending modulus increased from 87.55 GPa to 124.35 GPa and the bending strength increased from 621.63 MPa to 634.20 MPa) .

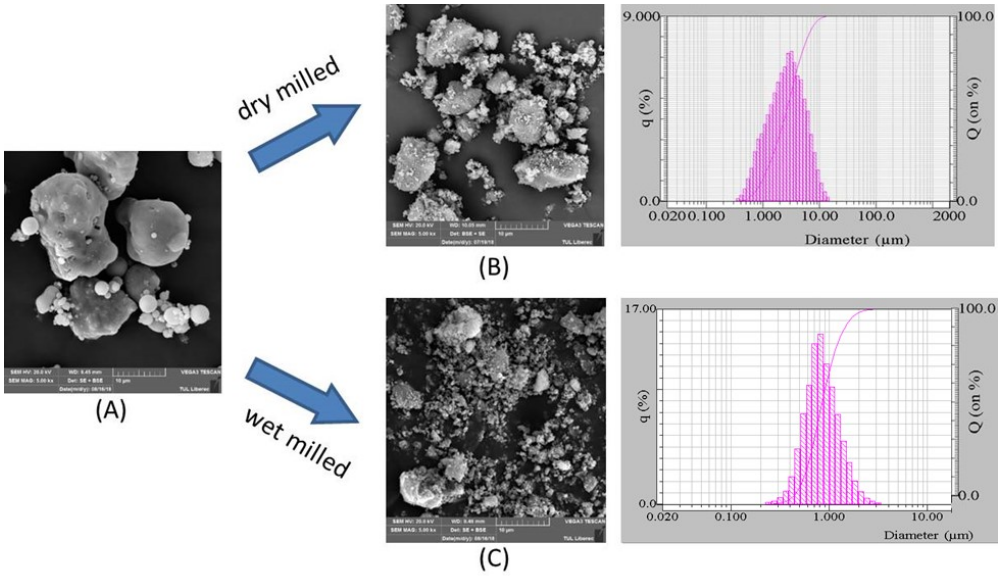

Fig. 12 (a) SEM pictures and size distribution of fly ash (A) original, (B) dry milling, (C) wet milling

The addition of wet milled fly ash in 1, 3 and 5% by weight, the bending modulus changed by 0.71%, 42.50% and 58.93% and bending strengths of 12.05%, 33.58% and 47.35% relative to ash-free samples. The agglomeration of fly ash particles is likely to increase at higher concentrations in the composites. For hybrid tapes containing wet milled fly ash particles, an improvement in tensile characteristics up to 3% by weight of fly ashes was found. There is a significant increase in the modulus and a slight increase in tensile strength compared to ash-free composites. A maximum increase of the initial modulus from 27.32 GPa (ashless composite) to 48.22 GPa (a composite containing 3% by weight of wet milled fly ash) was achieved. Hybrid tapes filled with 1, 2, 3, 4 and 5 % by weight of wet milled fly ash had an impact strength increase of 17.20%, 60.71%, 31.18%, 23.62% and 18.86%. However, the hybrid tapes filled with original fly ash exhibited only 5.64%, 10.27%, 13.54%, 11.22% and 1.57% increase in impact strength compared to ash-free hybrid tapes.

4. 3 Modeling of Spreading process

Spreading geometry

The spreading of fibrous bundle by mechanical means was experimentally studied by Wilson [21]. In fig. 13 it is shown his experimental setup where the fiber bundle was fixed at one point (Y) and passed over a pair of rods; a weight was attached at the opposite end of the point (Z) to apply tension to the fiber bundle. The spreading of the filaments was achieved by series of reciprocating motion (forward/backward) till stable fiber spreading was obtained.

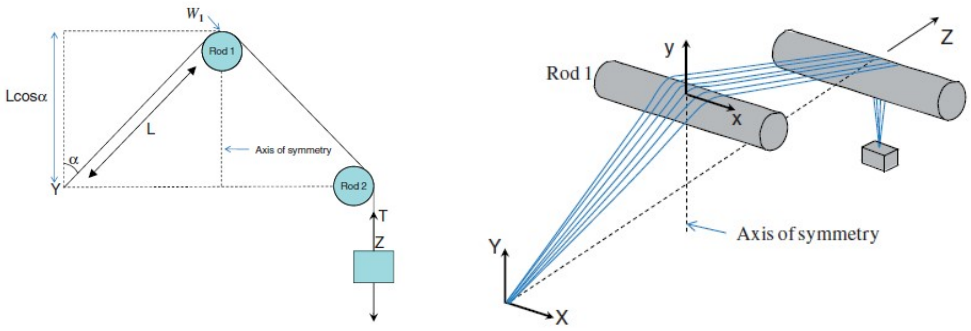

Fig. 13 Schematic illustration of the experimental setup to study lateral spreading of the individual filaments in a fiber bundle (adopted from [20])

The aggregate of the fibers in the bundle was assumed as a continuum and the width (a) of the bundle at the center of the first rod was predicted by eqn.

$$a = \sqrt[3]{12\ A\ L\ \cos\alpha} \qquad (1)$$

where A is the cross-sectional area of the bundle, α is the angle between the vertical and the anchor point (see fig. 13) and L is the length of the fiber bundle from the anchor point to the tangential contact point on the first rod. This model was extended to predict the mechanically induced spreading of E-glass fiber bundles [20].

Model of spreading process

The cross section geometry of spread tow composed from circular fibers can be predicted from idealized structural arrangements. The simple idealized model of spreading process is based on the assumption of limit honeycomb arrangement of fibers in tow cross section. In close honeycomb structure are filaments arranged in hexagonal concentric layers (see fig. 14).

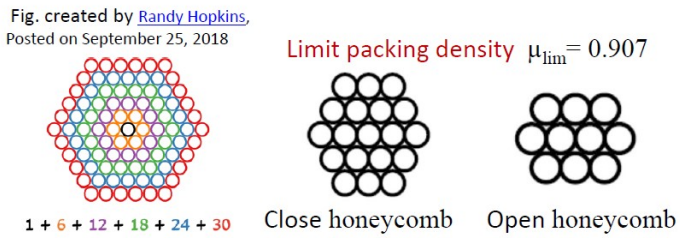

Fig. 14 Honeycomb structure

In the first concentric layer of this structure is only one filament, in the second layer is 6 filaments and in the i - th layer $i = 2,3,\ldots$ is number of filaments equal to $m_i = 6\ (i - 1)$. The structure containing l layers is composed from total $n = 3\ l^2 - 3\ l + 1$ filaments. Number of layers l_n in close honeycomb structure is related to the total number of filaments n.

$$l_n = 0.5 + \sqrt{n/3 - 1/12} \qquad (2)$$

Diameter D_n of circle with the same area as is area circumscribed to close honeycomb structure composed from filaments with diameter d is

$$D_n = 2\,d\left[\sqrt{n/3 - 1/12} - 0{,}5 + 1/\left(2\cos\ 30^o\right)\right]\sqrt{3\cos\ 30^o/\pi} \qquad (3)$$

In tow having the fineness T [tex] composed from individual filaments with fineness t [tex] is total number of filaments $n_T = T/t$. If $n_T = n$ the tow can ideally follow full close honeycomb structure.
Fineness of tow T is product of cross section area of filaments S and glass density ρ. The diameter D_T [mm] of ideal circular tow is then expressed in the form

$$D_T = \sqrt{\frac{4\,T}{\pi\ \mu\ \rho}} \qquad (4)$$

Here the packing density for compact honeycomb structure is $\mu = \mu_{lim} = 0{,}907$ and for real filaments is μ about 0,7. For tow with fineness 1200 tex and glass density ρ = 2580 kg m^{-3} is then for compact honeycomb D_T = 0,808 mm and for real multufilaments D_T = 0,9198 mm.
During flattening the closest possible arrangement according to the compact honeycomb structure is maintained (see fig. 15).

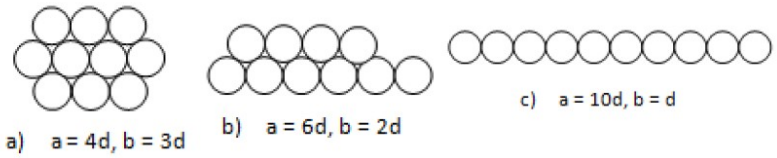

Fig. 15 Idealized spreading process

The width of the multifilament a and thickness b are varied depending on number of layers. Relative width α, relative thickness β and relative flatness γ ($\gamma \geq 1$) are defined as

$$\alpha = a/D_T \qquad \beta = b/D_T \qquad \gamma = \alpha/\beta = a/b$$

There are two types of geometrical assumptions of spreading leading to the prediction of relation between relative width and relative thickness.
A. Assumption of constant area during spreading in combination with Kemp racetrack cross section of tape leads to relation [20]

$$\alpha = \left[\pi/4 - \beta^2\left(\pi/4 - 1\right)\right]/\beta \qquad (5)$$

B. Assumption of constant perimeter during spreading in combination with Kemp racetrack cross section of tape leads to relation [20]

$$\alpha = \left[\pi - \beta(\pi - 2)\right] / 2 \qquad (6)$$

The dependence of α on β calculated from eqn. (5) and eqn. (6) are shown as curves in fig. 16.

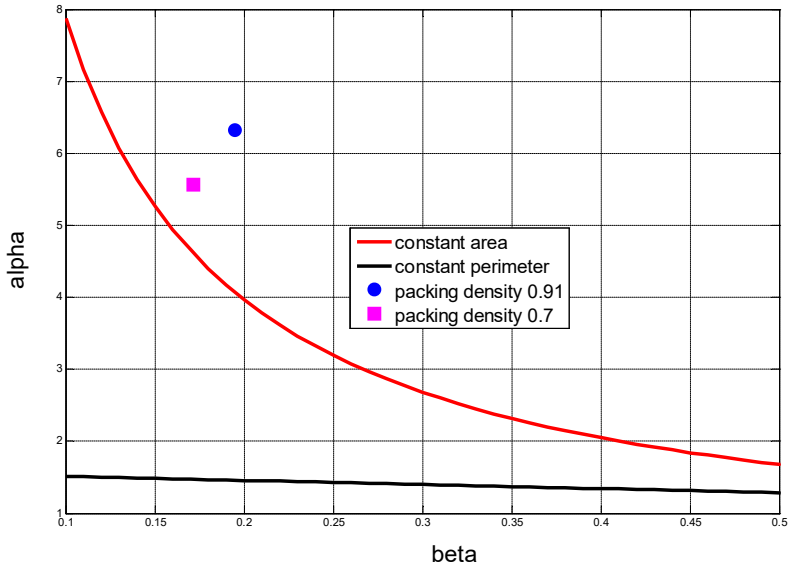

Fig. 16 Dependence of tape width on thickness under different assumptions

Let we have tow of fineness 1200 tex composed from 2376 filaments with close honeycomb structure. From eqn. 2 is total number of layers 29 including central one. In the outer 29 th layer is 107 filaments. The diameter of tow for compact honeycomb D_T = 0,808 mm and for real multifilaments D_T = 0,9198 mm. For fineness of filament 0,505 tex is corresponding diameter 0,0159 mm. Let the spread tow has the same shape characteristics as tow SL (see tab. 5). The corresponding relative width and thickness for both packing densities are given in the tab 5.

Table 5 Geometry of SL

Material	*Width a [mm]*	*Thickness b [mm]*	D_T *[mm]*	α	β	α_c
SLT μ= 0,9	5,122	0,158	0,81	6,34	0,196	4,05
SLT μ= 0,7	5,122	0,158	0,92	5,57	0,172	4,603

Based on the assumption of constant area during spreading are for β = 0, 196 and 0,172 calculated width α_c from eqn. (5). It is visible that for μ= 0,7 are α and α_c much closer (see also points in fig 16).

5. GEOMETRY OF MATERIALS

The geometrical characterization can be made by direct measurements or by using some special information as is fineness in unit tex. There are a lot of different derived units for description of geometry of fibers yarns, tows and tapes and therefore for simplicity of calculation are used these special derived units.

5.1 Fibers geometry

Typical fiber form is shown on fig. 17.

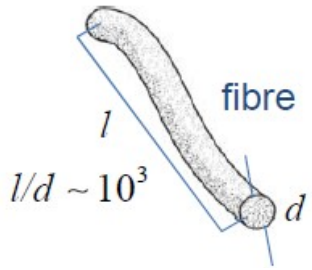

Fig. 17 Typical fiber with circular cross section of diameter d and length l.

It is obvious that fiber diameter d [μm] has dimension in microns, corresponding cross section area is S [μm^2], fiber length l [cm] has dimension in centimeters and fiber mass m [mg] is in miligrams. Basic characteristics of solids is relative mass expressed as density ρ [kg m^{-3}] where

$$\rho\left[\text{kg m}^{-3}\right] = \frac{mass\ [\text{kg}]}{Volume\left[\text{m}^3\right]} = 10^8 \frac{m}{S\,l} \qquad (7)$$

Density of fibers is then ratio between fiber mass m and fiber volume V as product of fiber cross section area S and length l.
In the case of linear fibrous structures, there are real limitations due to restricted cross section area and relative mass is better expressed as fineness T_f [tex] defined as

$$T_f\ [\text{tex}] = \frac{mass\ [\text{g}]}{length\ [\text{km}]} = 100\frac{m}{l} = 10^{-6}\rho\, S \qquad (8)$$

For estimation of fiber diameter in the case of circular cross section, it is possible to realize direct measurement from microscopic images of longitudinal fibers (see. fig. 18, for the fibers CH).

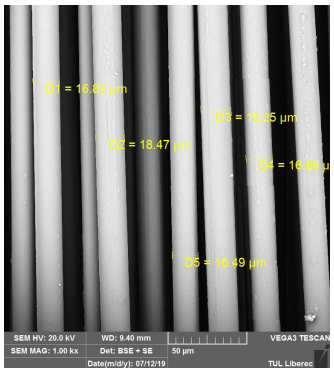

Fig. 18 Longitudinal portions of fibers CH and diameter evaluation

The fiber fineness T_f can be measured by nondestructive manner on device Vibroscope attached to tensile testing machine Fibrodyn. Principle of fineness measurement is forced vibrations. Results of measurements are given in tab. 6.
For checking of normality the so called **normal probability plot** is useful. The sample data is sorted in ascending manner and plotted on the x-axis. The y-axis represents the quantiles of the normal distribution, converted into probability values. Therefore, the y-axis scaling is not linear. Where the x-axis value is the i th sorted value from a sample of size N, the y-axis value is the midpoint between evaluation points of the empirical cumulative distribution function of the data. In the case of uncensored data, the midpoint is equal to $(i-0.5)/N$. Straight line in this graph is indication of normality [38]. Normal probability plot of fineness data for filaments from SL and CH filaments are shown in fig. 19.

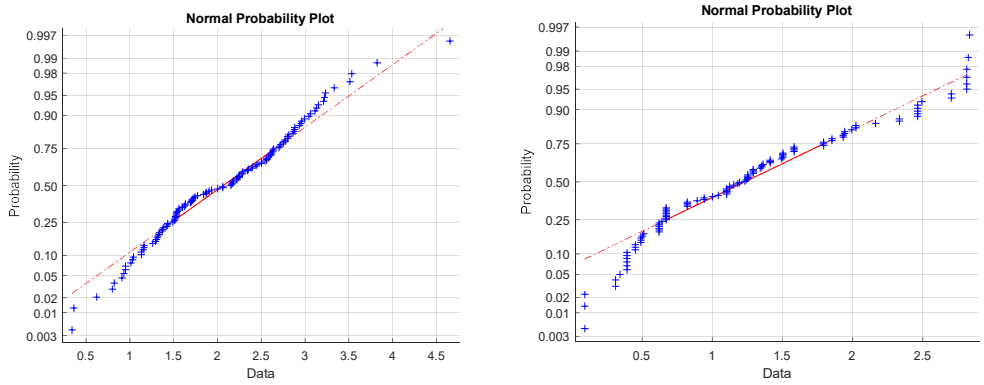

a) b)

Fig. 19 Checking of normality of fineness data for a) CH filaments, b) SL filaments

For the glass fibers of group CH was evaluated mean fineness from 100 direct measurements by Vibroscope T_f = 0,569 tex (95 % th confidence interval 0,490 – 0,519) and for glass fibers of group SL it was T_f = 0,505 tex (95 % th confidence interval 0,555 – 0,583).
It can be simply shown that circular fiber diameter d is related to fiber fineness by equation

$$d = \sqrt{10^6 \frac{4\ T_f}{\pi\ \rho_f}} \qquad (9)$$

From eqn. (9) is then mean diameter of glass fibers of group CH equal to 16,757 μm and mean diameter of glass fibers of group SL is equal to 15,787 μm. Mass of 5 cm portion of glass fiber of group CH computed from eqn. (7) is 0,0285 mg and for glass fiber of group SL it is 0,0253 mg. Basic geometrical characteristics of glass filaments are given in tab. 6.

Table 6. Geometry of filaments

material	*Fineness [tex]*	*diameter [μm]*	*Cross section area [μm²]*
Filaments CH	0,569	16,757	220,62
Filaments SL	0,505	15,787	195,82

5.2 Tows geometry

For geometric characterization of tows with rectangular cross-section were directly measured width b [mm] and thickness t [mm] and by weighting it was evaluated mass m_t [g] of l_t = 5 cm length portions. Results are summarized in tab. 7

Table 7. Geometry of tows

material	b [mm]	t [mm]	m_t [g]	N [-]	ρ_t [kg m^{-3}]	P_d [-]
CH	6,736	0,256	0,1234	4337,43	0,561	0,561
SL	5,122	0,158	0,0594	2351,68	0,587	0.587

The tow fineness T_t can be directly calculated for measured mass m_t and corresponding length l_t according to relation

$$T_t = 10^5 \frac{m_t}{l_t} \qquad (10)$$

For tows CH is from eqn. (10) T_t = 2468 tex and for tows SL is from eqn. (10) T_t = 1187,6 tex. Number of fibers N (filaments) in tow is equal to ratio

$$N = \frac{T_t}{T_f} \qquad (11)$$

The packing density P_d (equal to volume fraction of fibers in volume of tow with cross section area $S_t = b\ t$) can be calculated from eqn. (12)

$$P_d = 10^{-6} \frac{\pi\ N\ d^2}{4\ b\ t} \qquad (12)$$

The mass m_t can be simply predicted from eqn. (13)

$$m_t = 10^{-5}\, t\, b\, l_t\, \rho\, P_t \qquad (13)$$

For tows CH is from (13) m_t = 0,1248 g and for tows SL is from eqn. (13) m_t = 0,0613 g. These values are very slightly over measured m_t (see tab. 2) and showing that in scale of 5 cm there are not significant deviations from ideal straight state (influencing of measured m_t). Knowing mass of individual fibers and total mass of tow it is possible to calculate the number of fibers in tow

$$N = 10^3 \frac{m_t}{m_f} \qquad (14)$$

For tows CH is from eqn. (14) N = 4329 and for tows SL is from eqn. (14) N = 2347. These values are very slightly smaller than numbers in tab. 7 calculated from ratio of fineness.

5.3 Tapes geometry

For tapes geometrical characterization it is possible to use the same geometry measurements as in the case of tows. There were directly measured width b_T [mm] and thickness t_T [mm] and by weighting it was evaluated mass m_T [g] of l_T = 5 cm length portions. Results are summarized in tab. 8.

Table 8. Geometry of tapes

material	b_T [mm]	t_T [mm]	m_T [g]	w_f [-]	ρ_T [kg m^{-3}]	v_f [-]
CH	3,206	0,266	0,04914	0,6	1477,10	0,3435
SL	5,72	0,222	0,07482	0,7952	2087,029	0,642

From mass of tape m_T and mass of glass fiber in tape $m_{fT} = 10^{-3} m_f$ N (for tapes SL m_{fT} = 0,0595 g) it is simple to calculate mass portion of glass fibers w_f as their ratio (see. tab. 8). Mass portion of CH tape was known (see. tab. 8). For calculation of volume portion of glass fiber is valid

$$v_f = \frac{w_f \rho_T}{\rho_f} = \frac{w_f \rho_r}{w_f \rho_r + \left(1 - w_f\right)\rho_f} \qquad (15)$$

where ρ_T is density of tape composed from phase of glass fibers (density ρ_f) and phase of resin (density ρ_r)

$$\rho_T = \frac{\rho_r \, \rho_f}{w_f \, \rho_r + \left(1 - w_f\right)\rho_f} \qquad (16)$$

For the case of tapes CH is density of resin (POP) equal to 900 kg m^{-3} and from eqn. (16) is density of tape equal to 1477,10 kg m^{-3}. Volume portion of glass fiber calculated form eqn. (15) is then 0,3435. For the case of SL it is simple to calculate volume potion of glass directly from definition as ratio of volumes. The volume of glass fiber V_t [mm^3] in the tow is the same as in the tape and then simply

$$V_f = 10^6 \frac{m_t}{\rho_f} \qquad (17)$$

For SL tape it is V_f = 23,0155 mm^3. The total volume of tape V_T [mm^3] is equal to product of b_T, t_T and l_T (50 mm). After substitution of values from tab. 8 it results V_T = 35, 85 mm^3. The volume portion of glass fiber is then ratio of volumes i.e. v_f = 0,642. The SL tape density ρ_T [kg m^{-3}] is simply

$$\rho_T = 10^6 \frac{m_T}{V_T} \qquad (18)$$

After substitution into eqn. (18) it results ρ_T = 2087, 029 kg m^{-3}. For the SL is density of cured epoxy resin unknown, but it is possible to calculate it now from eqn. (15). After substitution it results ρ_r = 1198, 1 [kg m^{-3}].

6. STRENGTH DISTRIBUTION

Let us start with straight fiber of cross section area S_o [μm^2] (diameter d_o) and length l_o. After applying the load F [cN], the fiber is extended to the length l and reduced to the area S or diameter d.

The engineering stress σ [GPa], engineering strain ε [%], and draw ratio λ [%] are defined by well-known equations

$$\sigma = 1000 \frac{F}{S_o} \qquad \varepsilon = 100 \frac{l - l_o}{l_o} = 100 \frac{\delta}{l_o} \qquad \lambda = \frac{l}{l_o} = 1 + \varepsilon \qquad (19)$$

For calculating strength of filament extracted from SL and CH tows their fineness T_f in tex is at disposal. The corresponding engineering stress σ [GPa] is then

$$\sigma = 10^{-5} \frac{F \, \rho}{T} \qquad (20)$$

Formula (20) is used in sequel for treatment of data obtained by tensile testing of individual filaments.
For selected tows (SL, CH) is the load F [N] and S_o is sum of filaments cross sections areas i.e. area of individual filament S_f (see tab 6) multiplied by number of filaments N (see eqn. (14)). After calculation the S_o = 0,461 mm^2 for SL and S_o = 0,954 mm^2 for CH results. These results are very similar to results obtained by multiplying of macroscopic area of tow cross section (rectangle) by packing density of filaments in tow (see tab. 7).
For tapes SLT and CHT it is possible to calculate directly cross sectional area S_o of cross section rectangles from real dimensions given in tab. 8.
The derivative of draw ratio is defined as $d\lambda = dl / l$. After integration the so called true strain ε_t can be obtained

$$\varepsilon_t = \int_{l_o}^{l} \frac{dl^*}{l^*} = ln(\lambda) = ln(1+\varepsilon) \qquad (21)$$

The important characteristics of material deformation is so called Poisson ratio ν, defined as ratio of the relative transversal deformation ε_T and relative longitudinal extension ε

$$\nu = -\frac{\varepsilon_T}{\varepsilon} \quad where \quad \varepsilon_T = \frac{d - d_o}{d_o} \qquad (21)$$

The change of cross section area is then

$$\frac{A}{A_o} = (1 - \nu\ \varepsilon)^2 \qquad (22)$$

and change of volume due to deformation is

$$\frac{V}{V_o} = (1 - \nu\ \varepsilon)^2\ (1 + \varepsilon) \qquad (23)$$

For rubber and rubber like materials there is not changed volume during deformation, V/Vo = 1 (incompressible material) and $\nu = 0.5$. For majority of fibrous forming materials is volume increased due to extension (V/Vo > 1) and then $\nu < 0.5$ (usually $0.2 \le \nu \le 0.45$).
It was found that for sufficiently small deformations the values computed for constant Poisson ratio ν are fully acceptable. The engineering stress σ_t can be then expressed in the form

$$\sigma_t = \frac{F}{A} = \frac{\sigma}{(1 - \nu\,\varepsilon)^2} \qquad (24)$$

Let there is linear true stress/true strain dependence $\sigma_t = E\,\varepsilon_t$ for materials with constant Poisson ratio during deformation. The corresponding engineering stress/ engineering strain diagram is a function

$$\sigma = E(1 - \nu\,\varepsilon)^2\, ln(1+\varepsilon) \qquad (25)$$

where E is initial modulus for true stress/strain dependence which is equal to initial modulus of the engineering stress strain curve. Shape of function (25) depends on the value of Poisson ratio.

It was experimentally proved that Poisson ratio decreased with increasing of tensile elongation [32].

6. 1 Prediction of filaments strength

Main aim of the modeling and statistical analysis is specification of strength distribution and corresponding parameter estimation based on the experimental strengths (σ_{fi}) i = 1.....N. Filaments separated manually from materials SL and CH were tested on tensile testing machine under standard conditions. The loads at break were measured at gauge length 10 mm at rate of extension 10 mm/min. Load data were transformed to the stresses at break σ_{fi} [GPa] (see eqn. (20)). The sample of 120 stresses at break values was used for analysis and estimation of parameters. Experimental strength distribution of filaments is shown in fig. 20.

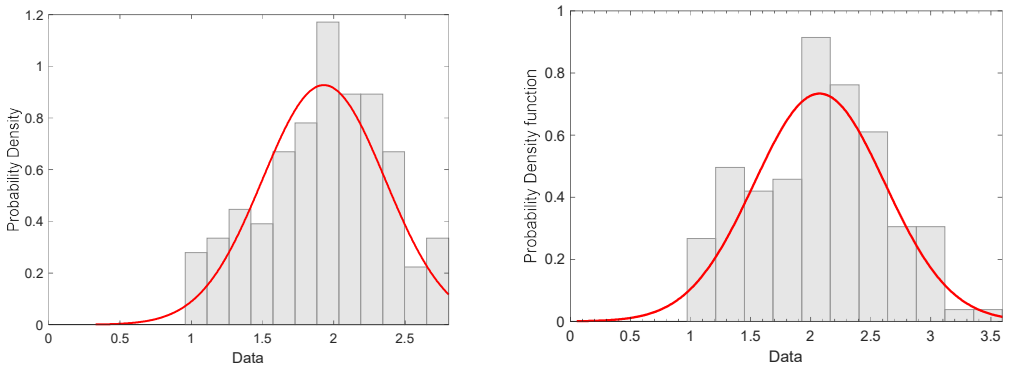

a) Material SL b) material CH

Fig. 20 Experimental strength distribution of filaments (red curve is probability density function of normal distribution)

Basic statistical characteristics of filament strength are given in tab. 9.

Table 9. Basic statistical characteristics of filaments strength

Material	*Mean* [GPa]	*Standard deviation* [GPa]	*Variation coefficient* [-]
Filaments CH	2,074	0,5459	26,323
Filaments SL	1,93	0,4318	22,3743

There is slightly higher strength of filaments from material CH in comparison with filaments from material SL. The normality plot (see. Fig. 21) is showing moderate systematic differences from assumption of data normality especially for filaments from tow SL.

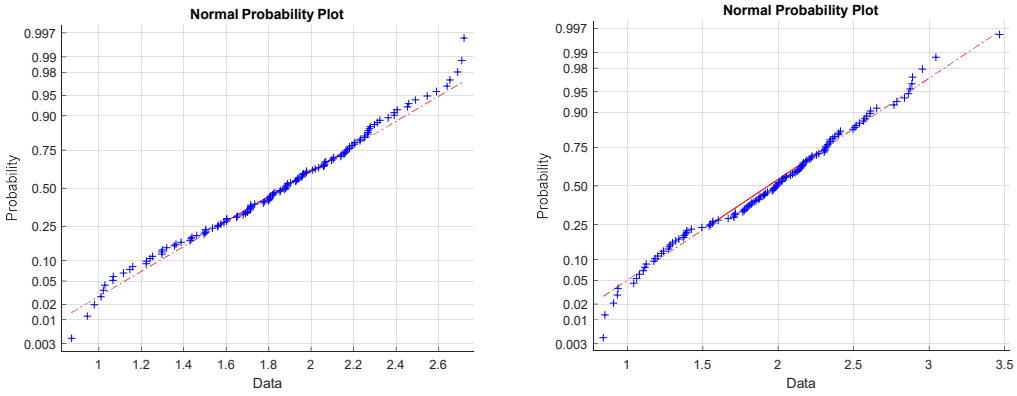

a) material SL b) material CH

Fig. 21 Normal probability plot of filaments strength (red line is probability ideal for normal distribution)

The fracture of fibers can be generally described by the micro mechanical models or on the base of pure probabilistic ideas [33]. The probabilistic approach is based on these assumptions:

(i) - fiber breaks at specific place with critical defect (catastrophic flaw),
(ii) - defects are distributed randomly along the length of fiber (model of Poisson marked process),
(iii) - fracture probabilities at individual places are mutually independent.

The cumulative probability of fracture $F(V, \sigma_f)$ depends on the tensile stress level and fiber volume V. The simple derivation of the stress at break distribution described for example by Kittl and Diaz [33] leads to the general form

$$F\left(V,\sigma_f\right) = 1-\exp\left(-R\left(\sigma_f\right)\right) \qquad (26)$$

The $R(\sigma_f)$ is known as the specific risk function. For famous Weibull distribution has function R the form [33]

$$R(\sigma_f) = \left(\frac{\sigma_f - A}{B} \right)^C \qquad (27)$$

Here A is lower strength limit (threshold), B is scale parameter and C is shape parameter (model WEI 3). For brittle materials is often assumed A = 0 (model WEI 2). Weibull models are physically no correct due to unsatisfactory upper limit of strength. More complicated risk functions were tested as well [34, 35], but based on the huge testing it has been determined that for basalt and glass fibers strength the 2 or 3 parameter Weibull distribution is suitable.

Probability density function (pdf) of 3 parameter Weibull distribution has the form

$$f(\sigma_f) = C\, B^{-C} (\sigma_f - A)^{C-1} \exp\left(-B^{-C} (\sigma_f - A)^C \right) \qquad (28)$$

Location parameter A is in fact the threshold value (for brittle materials is often A= 0), $B > 0$ is scale parameter and C is shape parameter. Weibull distribution is obviously denoted as $W(A, B, C)$. Changes of A causes shift of pdf on x axis. Changes of B have the similar meaning as changes of standard deviation in the case of normal distribution, i.e. express variability of data. Shape parameter C is responsible for changes of Weibull pdf form. For C > 1 is Weibull distribution unimodal and for B < 1 is pdf continuously decreasing with increasing of strength (exponential distribution). Influence of parameter C on the form of Weibull distribution is shown in fig. 22.

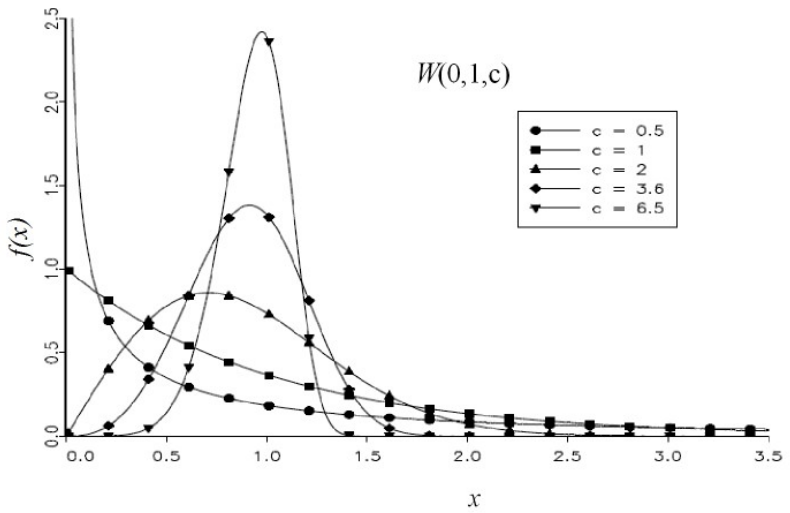

Fig. 22 Forms of Weibull distribution for different shape parameter C

Strength distribution of brittle materials obey often the two parameter Weibull distribution expressed in the alternative forms

$$F(\sigma_f) = 1 - \exp\left(-B_1\, l_f\, \sigma_f{}^C \right) \quad or \quad F(\sigma_f) = 1 - \exp\left(-(\sigma_f / B)^C \right) \qquad (29)$$

Scale parameter B is connected with filaments length l_f (gauge length) by relation

$$B = \frac{1}{\left(B_1\ l_f\right)^{1/C}} \qquad (30)$$

Different gauge lengths are influencing the parameter B only. If the measurements will be realized at length l_a it will be possible to calculate the corresponding parameter B_a from relation [36]

$$B_a = B\left(\frac{l_a}{l_f}\right)^{-1/C} \qquad (31)$$

The relation (31) corresponds to so-called size effect. Decreasing of gauge length will therefore increase the fiber strength.
The mean value $E(\sigma_f)$ and variance $D(\sigma_f)$ of fiber distribution are simple functions of parameters B and C only

$$E(\sigma_f) = B\ \Gamma\left(1+\frac{1}{C}\right) \qquad D(\sigma_f) = B^2\ \left[\Gamma\left(1+\frac{2}{C}\right) - \Gamma^2\left(1+\frac{1}{C}\right)\right] \qquad (32)$$

Gamma function $\Gamma(x)$ can be approximated by Stirling formula

$$\Gamma(z) \approx \sqrt{2\pi}\ z^{z-1/2} e^{-z} \exp\left[\frac{1}{12\ z} - \frac{1}{360\ z^3} + \frac{1}{1260\ z^5} - ...\right] \qquad (33)$$

Based on the Taylor expansion it is possible to use approximate relations

$$E(\sigma_f)/B \doteq 1 - \frac{0,57722}{C} + \frac{0,98905}{C^2} - ... \qquad (34)$$

and

$$D(\sigma_f) \doteq \frac{B^2\pi^2}{6\ C^2} \doteq 1,64493\ B^2/C^2 \qquad (35)$$

In the case of three parameter Weibull distribution with threshold A it is only necessary to add this quantity to mean value $E(\sigma_f)$.
In the tab. 10 are mean values $E(\sigma_f)$ and standard deviation $\sqrt{D(\sigma_f)}$ calculated from eqn. (31) by using Weibull distribution parameters (A, B, C) from tab. 10.

Table 10. Predicted basic statistical characteristics of filaments based on Weibull parameters

Material	*Mean pred.* [GPa]	*Standard deviation pred.* [GPa]
Filaments CH	2,074	0,5459
Filaments SL	1,93	0,4531

Comparing predicted values from tab. 10 with basic statistical characteristics from tab. 9 shows excellent agreement.

Other statistical characteristics of location are function of Weibull parameters. **Mode (**maximum on pdf) is equal to $M_o = B\ \left[(C-1)/C\right]^{1/C}$ and **median** is $x_{med} = B\ (\ln 2)^{1/C}$

For $C > 3$ or $C \doteq 1$ is approximately $\Gamma(x) = \left(1+\frac{1}{C}\right) \doteq 1$ and then $E(\sigma_f) \doteq B$. As C increases, the distribution is narrower, and is increasingly similar to the normal (Gaussian) distribution. Very interesting is expression of the coefficient of variation which is function of parameter *C* only

$$CV = \frac{\sqrt{D(\sigma_f)}}{E(\sigma_f)} = \left[\frac{\Gamma\left(1+\frac{2}{C}\right) - \Gamma^2\left(1+\frac{1}{C}\right)}{\Gamma^2\left(1+\frac{1}{C}\right)}\right]^{1/2} \qquad (36)$$

For higher *C* is then *CV* expressed in the simple form

$$CV = \frac{\pi}{C\sqrt{6}} = \frac{1.283}{C} \quad \text{for } \mathrm{C} \geq 10\,.$$

For small *C* is $CV = C^{-0.92}$ for $0.05 \leq \mathrm{C} \leq 0.5$. These approximations are interesting for interpretation of Weibull parameters as well.

At small loads – under small failure probability levels - the 'lower tail of the probability distribution can be used

$$F(\sigma_f) = 1 - \exp\left[-\left(\frac{\sigma_f}{B}\right)^C\right] \ \textit{approaches to}\ F(\sigma_f) \doteq \left(\frac{\sigma_f}{B}\right)^C \qquad (37)$$

This power law form of the fracture probability is a simple approximation at small loads. Estimation of Weibull parameters is obviously based on the experimental values σ_{f_i}, $i = 1...N$.

Standard statistical procedure for parameter estimation in statistical models is *maximum likelihood* (ML) method based on maximization of likelihood function. This method is very interesting because of its good statistical properties (asymptotic efficiency, consistency and asymptotic normality of estimators) [38]. For the case

when σ_{fi} , i = 1,...N are independent random variables with the same probability density function $f(\sigma)$ = $F'(\sigma_i, \mathbf{a})$ is the logarithm of likelihood function in the form

$$\ln L(\mathbf{a}) = \sum_{i=1}^{N} \ln\left(f\left(\sigma_{fi}, \mathbf{a}\right)\right) \qquad (38)$$

where **a** = (A, B, C) are parameters of corresponding probability density function. The MLE estimators **a*** can be obtained by the maximization of ln L(a). This task can be simply converted to the solving of the set of nonlinear equations (see [38]). In some cases is this task complicated and special technique should be used [38].

For rough parameter estimates of some above mentioned models the moment based method can be used. The main idea of this method is very simple. Based on the M sample moments and corresponding theoretical moments for selected strength distribution the M nonlinear equations can be created. *Simplest method of moments* is based on equating mean fiber strength $\bar{\sigma}_f$ and corresponding standard deviation s_f values computed by the standard manner and calculated from eqn. (32). In this case the parameter C is solution of from nonlinear equation

$$\bar{\sigma}_f \left(\frac{\Gamma\left(1+2/C\right)}{\Gamma^2\left(1+1/C\right)} - 1 \right)^{\frac{1}{2}} - s_f = 0 \quad \text{for} \quad C \in \langle 1;9 \rangle \qquad (39)$$

The parameter B is then evaluated from relation

$$E(\sigma_f) = \bar{\sigma}_f \text{ i.e. } B = \bar{\sigma}_f / \Gamma\left(1+\frac{1}{C}\right) \qquad (40)$$

The solution of nonlinear eqn. (39) for specified range of C is not in all cases successful.

Non iterative methods of moments is based on so called Weibull moments m_r defined by relations

$$m_r = \sum_{i=0}^{N-1} \left(1 - i/N\right)^r \left(\sigma_{f(i+1)} - \sigma_{f(i)}\right) \qquad (41)$$

Symbol $\sigma_{f(i)}$ means i th order statistics i.e. i th smallest value of breaking strength in sample. Therefore it should be $\sigma_{f(i)} \le \sigma_{f(i+1)}$. Order statistics can be simply obtained by sorting of experimental data in ascending order. For i = 0 is formally $\sigma_{f(0)} = 0$. This technique can be used for the rough estimation of strength distribution parameters. Shape parameter C can be estimated from relation [43].

$$C = \frac{\ln 2}{\ln\left(m_1 - m_2\right) - \ln\left(m_2 - m_4\right)} \tag{42}$$

For estimation of the threshold (lower limiting strength) A is valid

$$A = \frac{m_1\ m_4 - m_2^2}{m_1 + m_4 - 2m_2} \tag{43}$$

and estimate of scale parameter B is in the form

$$B = \frac{m_1 - A}{\Gamma\left(1+1/C\right)} \tag{44}$$

where Γ(x) is Gamma function. For two parameter Weibull model is $A = 0$ and C is estimated from relation

$$C = \frac{\ln 2}{\ln\left(m_1\right) - \ln\left(m_2\right)} \tag{45}$$

The assumption $A = 0$ is valid if the B and C estimates for two and three parameter Weibull model are reasonable close. The parameters A, B, C calculated from eqn. (42), (43), (44) are shown in tab. 11.

Table 11. Three parameter Weibull fit of filaments strength (Weibull moments)

material	*Threshold* A [GPa]	*Weibull shape* C [-]	*Weibull scale* B [GPa]
CH	0,1294	4,0115	2,1451
SL	0,0855	4,8664	2,0120

The predicted values of mean and standard deviation (see tab. 10) calculated from these parameters are very close to corresponding parameter calculated by standard manner (arithmetic mean and sample standard deviation).

Very attractive for quick parameter estimation is utilization of the so called *Q-Q* graph concept. *Q-Q* graph is suitable for the check of Weibull distribution acceptability for experimental data as well. This graph is simply derived from distribution function defined by eqn (26) replacing of $F\left(\sigma_{f_i}\right)$ by order probabilities $P_i = i/(N+1)$ for $i = 1..N$ and σ_{f_i} by ordered statistics $\sigma_{f(i)} \le \sigma_{f(i+1)}$. More precise is to use corrected order probabilities [38]

$$\mathrm{F}\left(\sigma_{\mathrm{fi}}\right) = P_{\mathrm{i}} = \frac{i - 0,5}{N + 0,25} \tag{46}$$

After substitution and rearrangements, the final model form results

$$ln\left[-ln\left(1-P_i\right)\right]=C\ \ ln\left(\sigma_{f(i)}-A\right)\ -\ C\ ln\left(B\right) \qquad (47)$$

The Q-Q graph is then dependence of $Y_i = \ln\left(-\ln\left(1-P_i\right)\right)$ on the $X_i = \ln(\sigma_{f(i)})$, i.e. nonlinear model

$$Y_i=C\ \ ln\left(X_i-A\right)\ -\ C\ ln\left(B\right) \qquad (48)$$

In the case of validity of Weibull two parameter distribution (A = 0) should be this dependence straight line with slope C and intercept – C ln(B). The parameter estimation is now converted into nonlinear regression problem. The parameter estimates A, B, C are then obtained by nonlinear least squares i.e. by minimizing of criterion

$$S=\sum_{i=1}^{N}\left[y_i-C\ \ ln\left(X_i-A\right)\ +\ D)\right]^2 \qquad (49)$$

Here parameter $D = C$ ln (B). Transformation of parameter estimation problems to the regression problem enables to use the statistical criteria for selection of the optimal model form (e.g. 2 or 3 parameter Weibull distribution). Suitable is Akaike information criterion AIC defined as [38]

$$AIC=N\ln\ \left(S^*/N\right)+2\ M \qquad (50)$$

For graphical evaluation of usefulness of Weibull distribution, the corrected Weibull QQ plot can be simply constructed. This plot is using eqn. (47) where is A replaced by estimator from eqn. (42). Linearity in this graph is showing full acceptability of Weibull distribution. Corrected Weibull QQ plot of filaments strength distribution is shown in fig. 23.

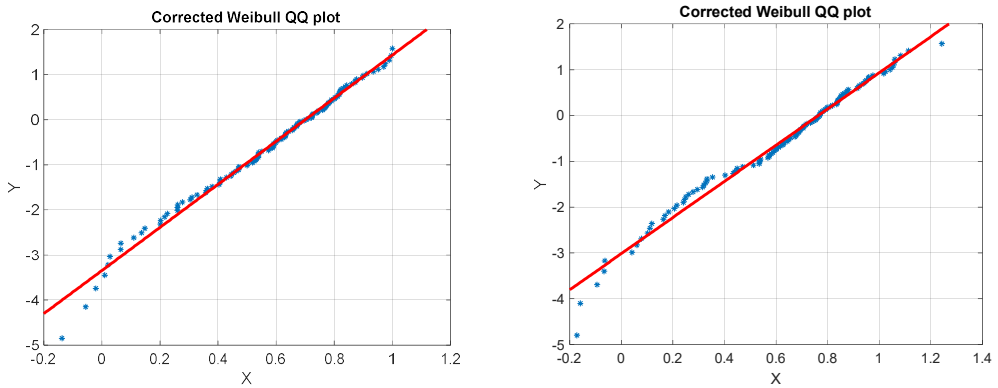

a) material SL b) material CH

Fig. 23 Corrected Weibull QQ plot of filaments strength distribution (red line is ideal for Weibull distribution)

Other simple estimate of threshold value of breaking strength A is based on the extreme order statistics [45]

$$\hat{A} = \left(\sigma_{f(1)}\ \sigma_{f(N)} - \sigma_{f(2)}^2\right) / \left(\sigma_{f(1)} + \sigma_{f(N)} - \sigma_{f(2)}\right) \qquad (51)$$

In some situations, the bundle (roving) strength can be evaluated more easily. A lot of works is devoted to evaluation of the single fiber strength distribution from fiber bundle strength. The main assumptions are [40]:

1. Single fiber exhibits the unimodal (usually Weibull type) strength distribution.
2. Stress-strain dependence of single fiber is linear with constant of proportionality named elastic modulus E_f.
3. Distribution of the elastic modulus is independent on the distribution of the strain at break of individual fibers.
4. The applied load is distributed uniformly among the surviving fibers at any instant during a tensile test.

Let $F(\varepsilon)$ is the failure probability for a single fiber strained to value $\varepsilon = \sigma / E_f$ and below, N_o is the initial number of fibers in bundle and E_f is the mean value of fiber elastic modulus. The number of surviving fibers is then equal to [40]

$$N = N_o\ (1 - F(\varepsilon)) \qquad (52)$$

The corresponding stress in fiber bundle is [36]

$$\sigma_B = N_o\ \varepsilon\ E_f\ (1 - F(\varepsilon)) \qquad (53)$$

Strain ε_M at the maximal bundle stress σ_M can be obtained from derivative of eqn. (53). After rearrangements the final relation has the form [36]

$$\varepsilon_M = \frac{(1 - F(\varepsilon_M))}{p(\varepsilon_M)} \qquad (54)$$

where $p(\varepsilon_M)$ is single fiber failure probability density function. After substitution from eqn. (54) to eqn. (53) the relationship between maximum bundle stress σ_M, corresponding bundle strain ε_M and fiber strain distribution results

$$\sigma_M = N_o\ \varepsilon_M\ E_f\ (1 - F(\varepsilon_M, \mathbf{a})) = \frac{N_o\ E_f\ (1 - F(\varepsilon_M, \mathbf{a})^2}{p(\varepsilon_M, \mathbf{a})} \qquad (55)$$

For known type of individual fibers elongation at break distribution $F(\varepsilon, \mathbf{a})$ it is then possible to estimate corresponding parameters $\boldsymbol{a}$ by using of nonlinear regression. Denote that $\boldsymbol{a}$ is set of parameters describing distribution of break (for Weibull distribution $\boldsymbol{a} = (A, B, C)$).

6.2 Prediction of parallel fibrous bundle strength

Tows can be treated as parallel fibrous bundles. For modeling of parallel bundle of filaments (fibers) the following assumptions are frequently used [36, 37, 42]:

1. The single fiber strength is unimodal and obeys two parameter Weibull distribution.
2. Stress-strain dependence of single fiber is linear with constant of proportionality named elastic modulus E_f,
3. Distribution of the elastic modulus is independent on the distribution of the strain at break of individual fibers (or is simply constant).
4. Fibrous bundle is composed from N_f straight parallel fibers clamped at both ends.
5. When a fiber breaks, the load is carryings by survived fibers (distributed equally among the rest of fibers).
6. The changes of bundle geometry and dimensions during extension are neglected.

From assumption that the *applied load* is shared equally between the fibers the basic relations between single fiber and fibrous bundle can be expressed [36]. Starting is comparison of quantiles estimated as *order statistics*. Fibrous bundle quantiles are defined as $\sigma_{B(1)} \le \sigma_{B(1)} \le .... \le \sigma_{B(N)}$, where $\sigma_{B(i)}$ is i-th smallest bundle strength in the sample of N bundles.. Fibrous bundle quantiles are defined as $\sigma_{f(1)} \le ... \le \sigma_{f(i)} \le \sigma_{f(i+1)} \le ...\sigma_{f(Nf)}$ in the same manner.

The stable bundle (with one break only) is defined by the following relation between quantiles

$$\sigma_{B(i)} \le \sigma_{f(1\,-\,i/N)} \le \sigma_{B(i+1)}$$

For micromechanical fibrous bundle model is the average load on a fiber F/N_{f} at a given strain $\varepsilon = \sigma / E_{\mathrm{f}}$ equal to [37]

$$\frac{F}{N_f} = \varepsilon\left(1 - F(\varepsilon)\right) + a\ \varepsilon F(\varepsilon) \qquad (56)$$

where F [N] is total load and $0 < a < 1$ is factor of reducing stiffness of fibers at the failure point [37]. At a given deformation ε the fibers with breaking thresholds $\sigma_{\mathrm{in}} < E_f\ \varepsilon$ are broken. All other fibers keep the equal stress $E_f\ \varepsilon$. Hence, the macroscopic constitutive behavior σ(ε) of the bundle can be expressed in the form [37]

$$\sigma\left(\varepsilon\right) = E_f \varepsilon\left(1 - F(\varepsilon)\right) \qquad (57)$$

where $(1 - F(E_f \varepsilon))$ is the portion of survived fibers at the deformation ε. For large fibrous bundles it is possible to assume that at fixed strain $\varepsilon = \sigma/E_f$, the number of surviving fibers, $N_B(\sigma)$, follows a binomial distribution with mean $N_f \; p(\sigma)$ and variance $N_f \; p(\sigma) \; (1- p(\sigma))$, where $p(\sigma)=1 - F(\sigma)$ [36].
The bundle stress, σ_B has mean $\sigma_f \; p(\sigma_f)$ and variance $\sigma_f^2 \; p(\sigma_f)(1-p(\sigma_f))/N_f$.
Simple approach for prediction of parallel fibrous bundle strength modeling is used in the works [36, 41, 42]. The computation has two stages:

1. Estimation of fiber Weibull parameters from experimental mean strength and standard deviation.
2. Estimation of parallel fibrous bundle of fibers strength.

Let the fiber distribution is Weibull two-parameter type and scale parameter A and shape parameter C are calculated from mean fiber strength $\bar{\sigma}_f$ and corresponding standard deviation s_f by using eqn. (39) and (40) or by Weibull moments.
For the computation of fibrous bundles distribution, it is then possible to use famous Daniel's result, that for large bundles (number of fibers in cross section N_f is more than 100) is bundle strength approaching to normal distribution [44]

$$H\left(\sigma_B\right) = \frac{1}{\sqrt{2\pi}.s_B} \exp\left[-\frac{\left(\sigma_B - \bar{\sigma}_B\right)^2}{2{s_B}^2} \right] \tag{58}$$

Mean strength of fibrous bundle $\bar{\sigma}_B$ is equal to [39]

$$\bar{\sigma}_B = B\left(C \exp(1)\right)^{-\frac{1}{C}} \tag{59}$$

Corresponding standard deviation s_b is

$$s_B = \left(B / \sqrt{N_f}\right) \; C^{-1/C} \sqrt{exp\left(-1/C\right)\left(1 - exp\left(-1/C\right)\right)} \tag{60}$$

The corrected mean strength of fibrous bundle $\bar{\sigma}_{Bc}$ is [36]

$$\bar{\sigma}_{Bc} = \bar{\sigma}_B \left(1 + 0.99 N_f^{-2/3} \left(\exp(2/C)/C\right)\right)^{1/3} \tag{61}$$

and corrected standard deviation s_{bc} is

$$s_{Bc} = s_B \sqrt{1 - 0.317 \left(\bar{\sigma}_B / s_B\right)^2 \left(\exp(2/C) / \left(N_f C\right)\right)^{2/3}} \tag{62}$$

In the tab. 12 are calculated mean bundle strength $\bar{\sigma}_{Bc}$ and corresponding standard deviations s_{bc} from parameters of filament strengths Weibull distribution (see tab. 11)

Table 12. Three parameter Weibull fit of filaments strength (Weibull moments)

Material	*Mean pred.* [GPa]	*Standard deviation pred.* [GPa]
tow CH	1.1858	0.0096
tow SL	1.1835	0.0117

In comparison with experimental results (see tab. 13) it is visible moderate agreement of mean values but predicated standard deviations are highly underestimated.
The factor of fiber strength utilization in bundle is defined by relation

$$\phi = \frac{\bar{\sigma}_B}{\bar{\sigma}_f} \qquad (63)$$

For the case of Weibull distribution of fiber strength and normal distribution of bundle strength the simple approximate relation for utilization of fiber strength in bundle was derived [39].

$$\phi = u^u \exp(-u)/\Gamma(1+u) \quad \textit{where} \quad u = 0,909\,\mathrm{CV}_f \qquad (64)$$

In eqn. (64) is CV_f variation coefficient of fiber strength (see eqn. (36)). It is interesting that utilization of fiber strength in bundle is function variation coefficient of fiber strength only. In fig. 24 is solid line computed according to eqn. (62) and dashed line is computed by approximate relation (63). For example, fiber strength variation coefficient 30 - 40% corresponds to utilization of fiber strength in bundle 0,54 - 0,60. In Fig. 24 the point of 35% fiber strength variation coefficient and 0,56 utilization of fiber strength in bundle is marked by circle.

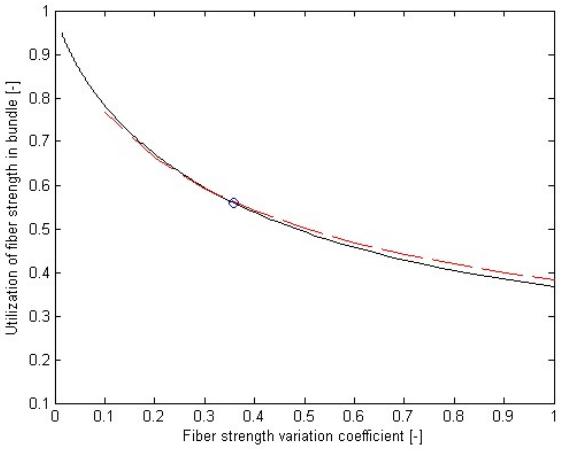

Fig. 24 Utilization of fiber strength in bundle

Tows SL and CH were tested on tensile testing machine under standard conditions. The loads at break were measured at gauge length 200 mm. Load data were transformed to the stresses at break σ_{Bi} [GPa]. The sample of 120 stresses at break

values was used for analysis and estimation of parameters for both tows. Basic statistical characteristics of tow strength are given in tab. 13.

Table 13. Characteristics of tow strength (moments Weibull)

material	*Mean* [GPa]	*Standard deviation* [GPa]	*Threshold* A [GPa]	*Weibull shape C* [-]	*Weibull scale B* [GPa]
CH	1,2817	0,1398	0,8886	3,0903	0,4396
SL	0,8845	0,1106	0,5737	3,0970	0,3475

Experimental tow strength distribution of filaments is shown in fig. 25.

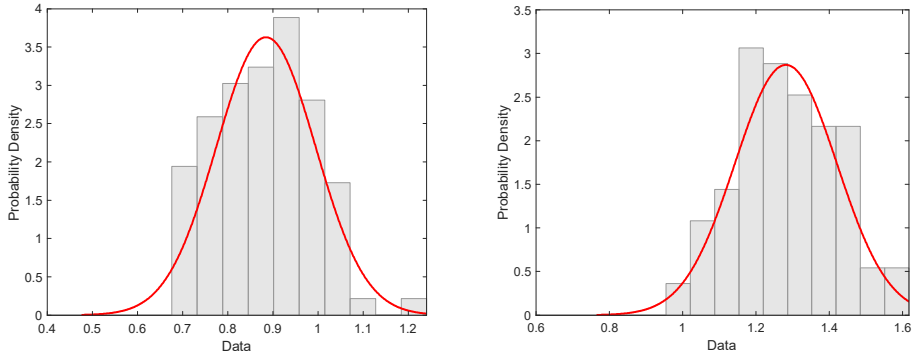

a) material SL b) material CH

Fig. 25 Experimental strength distribution of tows (red curve is probability density function of normal distribution)

There is much higher strength of material CH in comparison with material SL. The normal probability plots (see Fig. 26) are showing moderate tails differences from assumption of data normality. This differences are much higher for tow SL.

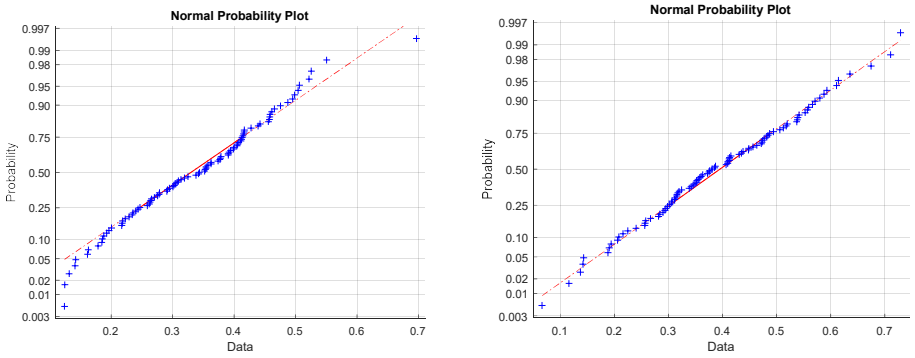

a) material SL b) material CH

Fig. 26 Normal probability plot of tows strengths (red line is probability ideal for normal distribution)

Relatively big decrease of tow strength in comparison with filaments strength is partially caused by filaments bundle curling leading to filament waviness. For expressing of waviness influence on stiffness the knock-down factor, *kd*, for a wavy filaments (idealized as the curved beam wit modulus E_1) related to that of a straight

filaments (idealized as the straight beam with modulus E_0) as, $kd = E_1 / E_0$ (see fig. 27) [46].

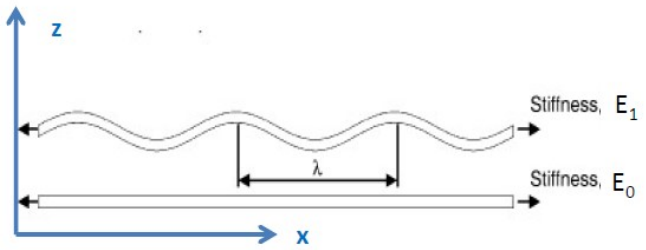

Fig. 27 Idealized filament waviness in tow (adopted from [46])

Magnitude k_d depends on magnitude and wavelength of wavy pattern and ca be modeled as sinusoidal curve.

$$z = A \sin\left(\frac{2\pi}{\lambda} x\right) \tag{65}$$

where λ is the crimp wavelength A is amplitude (related to standard deviation SD of z) $A = SD\sqrt{2}$ [46]. For A = 60 μm, λ = 2,5 mm is kd = 0.9. Waviness is probably higher for SL tow (see figs 1e and 2c).
Corrected Weibull QQ plot of tow strength distribution is shown in fig. 23.

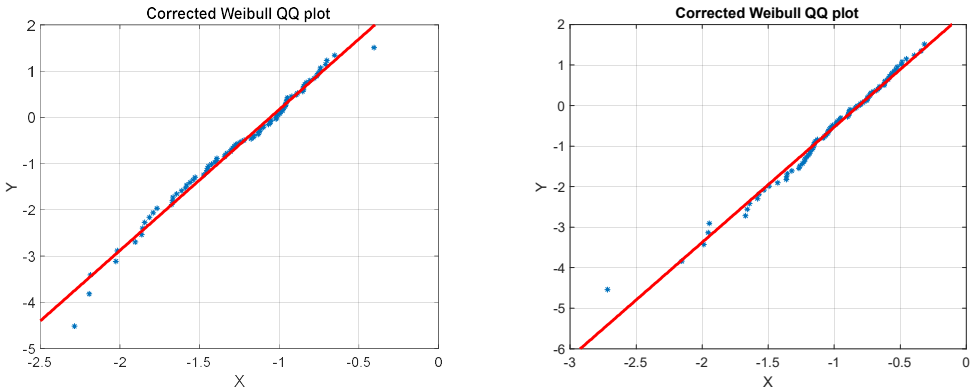

Fig. 28 Corrected Weibull QQ plot of tow strength (red line is ideal for Weibull distribution)

The deviation from Weibull distribution on the tails part are clearly visible.

6.3 Prediction of tapes strength

Tapes SLT and CHT were tested on tensile testing machine under standard conditions. The loads at break were measured at gauge length 200 mm. Load data were transformed to the stresses at break σ_{Bi} [GPa]. The sample of 120 measurements was used for analysis and estimation of parameters. Basic statistical characteristics of tape strength are given in tab. 14.

Table 14. Characteristics of tape strength (moments Weibull)

material	*Mean* [GPa]	*Standard deviation* [GPa]	*Threshold* A [GPa]	*Weibull shape C* [-]	*Weibull scale B* [GPa]
CHT	0,387	0,0429	0,275	2,84	0,126
SLT	1,0643	0,184	0,3591	4,49	0,7739

The mean strength of SLT is over the mean strength of SL (0,885 GPa) which indicates validity of mixture rules (composite strength exceed strength of strongest constituent). The strength of CHT is very small in comparison with strength of SLT and therefore the hybrid tape with epoxy resin is much better that tape with polypropylene component.

Experimental strength distribution of tapes is shown in fig. 29.

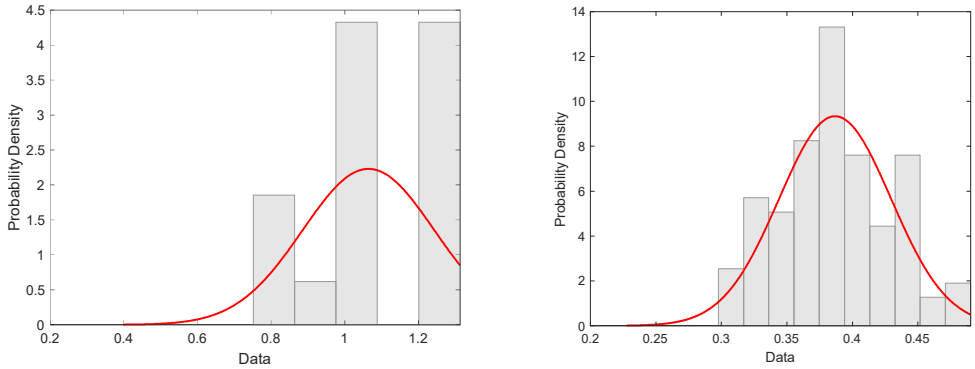

a) material SLT b) material CHT

Fig. 29 Experimental strength distribution of tapes (red curve is probability density function of normal distribution)

Due to the small sample size of SLT is piece-wise constant nonparametric estimator of probability density function based on the histogram not very useful. The normal probability plot (see Fig. 30) is showing moderate tails differences from assumption of data normality for both tapes. This differences are much higher for tape SL with very small sample size.

Assuming the filaments have lower breaking elongation, the tape strength can be predicted from simple mixture rule

$$\sigma_T = v_f \ \sigma_B + \left(1 - v_f\right) E_m \ \varepsilon_B \qquad (66)$$

where E_m is the matrix modulus, v_f is the volume fractions of the fiber and ε_B is the breaking strain of the fiber bundle, which is related to the bundle strength $\sigma_B = E_f \varepsilon_B$ where the tensile modulus of the bundle is identical to that of the fiber.

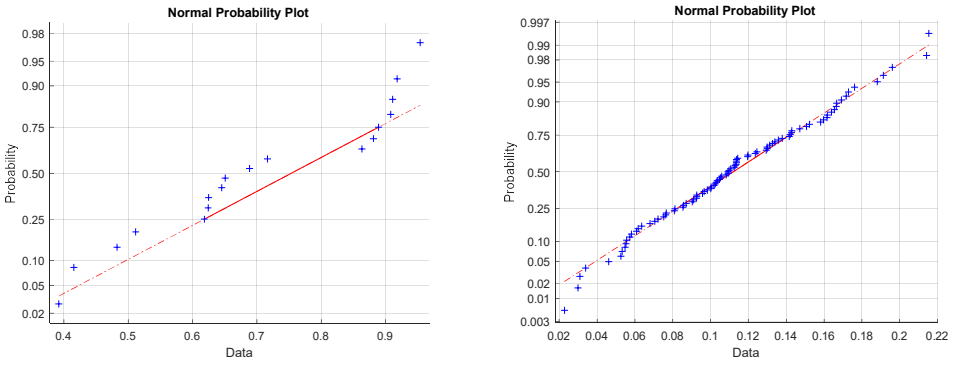

a) material SL b) material CH

Fig. 30 Normal probability plot of tows (red line is probability ideal for normal distribution)

The tape strength σ_T (eqn. (65)) is sum of contribution of fibrous phase σ_{Tf} and matrix phase σ_{TM}

$$\sigma_T = \sigma_{Tf} + \sigma_{TM} = v_f \ \sigma_B + \left(1 - v_f\right) \frac{E_m}{E_f} \ \sigma_B \qquad (67)$$

The contributions of fiber ($v_f = 0{,}642$) and matrix phases to the tape strength are given in tab. 15

Table 15 Components of tape strength

material	*Tape* $\bar{\sigma}_T$ [GPa]	*Fiber* $\bar{\sigma}_T$ [GPa]	*Matrix* $\bar{\sigma}_T$ [GPa]	E_m/E_f
SLT	1,0643	0,5677	0,4966	0,1778

Due to the normality of σ_B is σ_T as well normally distributed and for mean $\bar{\sigma}_T$ is valid [41]

$$\bar{\sigma}_T = \left(v_f + \frac{\left(1 - v_f\right) E_m}{E_f} \right) \bar{\sigma}_B \qquad (68)$$

Corresponding standard deviation s_T has the form

$$s_T = \left(v_f + \frac{\left(1 - v_f\right) E_m}{E_f} \right) s_B \qquad (69)$$

where $\bar{\sigma}_B$ and s_B are the mean fiber bundle strength and its standard deviation which can be calculated from eqn (32).

In the case of no validity of mixture rule it is possible to adopt hypothesis than filaments can be broken in matrix phase repeatedly into smaller parts till their length will be over critical length l_c [41]

$$l_c = \left(\frac{r_f \left(\frac{4}{3} \; B \right) \Gamma \left(1 + \frac{1}{C} \right)}{\tau_y} \right)^{C/(1+C)} \tag{70}$$

where r_f is the fiber radius and τ_y is the yielding shear strength of the matrix adjacent to the interface or that of the fiber-matrix interface, whichever is less This modification is crucial so that the effect of fiber-matrix interaction can be included. The mean $\bar{\sigma}_T$ and standard deviation s_T of tape strength can be calculated fron eqn (67) and (68) replacing bundle strength and standard deviation by $\bar{\sigma}_B(l_c)$ and $s_B(l_c)$ by modification of parameter B due to different length (replacing l_f by the critical length l_c or using eqn. (31) for calculating B_a).

7. CONCLUSION

The proper equations for geometrical characteristics of filaments, tows and tapes were compiled and used for selected materials. It was observed by SEM that the glass filaments in hybrid tapes SLT are uniformly dispersed in the epoxy resin material and the interface compatibility is good. The strength distribution of filaments was successfully modeled by Weibull distribution. The strength distribution of tows and bundles was described by Weibull distribution as well. For predictive purposes the basic strength distribution parameters (mean and standard deviation) were calculated from Weibull distribution parameters (A, B, C) of filaments. It was found that hybrid tape SLT has superior tensile mechanical behavior.

8. ACKNOWLEDGEMENT

This work was supported by the Ministry of Education, Youth and Sports of the Czech Republic and the European Union - European Structural and Investment Funds in the frames of Operational Programme Research, Development and Education - project Hybrid Materials for Hierarchical Structures (HyHi, Reg. No. CZ.02.1.01/0.0/0.0/16_019/0000843) and project "Sophisticated hybrid tapes for fabrication of composites by precise winding" (project identification no. TJ01000292) / Technology Agency of the Czech Republic (Programme Zeta).

9. REFERENCES

[1] Skoko M.: *Investigation of the Properties with Multiaxial Strengths and Deformations of Coated Fabrics*, Tekstil **7,** 339-344 (1998)

[2] Behera B.K., Hari P.K., Eds.: *Woven textile structure: Theory and applications.* Cornwall, UK: Woodhead 2010.

[3] Ohlsson F.: *Weight reduction by optimized reinforcement structures*, chap. 8 in book Njuguna J. ed.: *Lightweight Composite Structures in Transport Design*, Manufacturing, Analysis and Performance Elsevier Ltd., Cambridge 2016.

[4] Cornelissen B., Akkerman R.: *Towards Modeling of the Frictional Behavior of Deforming Fibrous Tows: A Geometrical Approach*, chap. book Binetruy Ch., Boussu F. eds: Recent Advances in Textile Composites , DEStech Publications, Inc., Lancaster 2010.

[5] Jones R. M.: *Mechanics of Composite Materials*, CRC Press, New York 2014

[6] EL-Dessouky H.M.: *Ultra-light weight thermoplastic composites: tow spreading technology*, ECCM15 – 15th European Conference on Composite Materials, Venice, Italy, 24-28 June 2012.

[7] Artemenko S. E.: *Polymer composite materials made from carbon, basalt, and glass fibres. Structure and properties.* Fibre Chem. **No.** 3, 226-229 (2003)

[8] Artemenko S.E., Kadykova Y. A.: *Polymer composite materials based on carbon, basalt, and glass fibres*, Fibre Chem., **No. 1** 37-39 (2008)

[9] Singha K.A.: *Short Review on Basalt Fibre*, Int. J. Text. Sci. **4**, 19-28 (2012)

[10] Cerny M., Glogar P., Golias V., Hruska J., Jakes P., Sucharda Z., Vavrova I.: *Comparison of mechanical properties and structural changes of continuous basalt and glass fibres at elevated temperatures,* Ceramics – Silikáty, **2**, 82-88 (2007)

[11] Militký J., Kovačič V., Bajzík V.: *Mechanical Properties of Basalt Filaments*, Fiber. Text. East. Eur. **15**, 49-53 (2007)

[12] Kovačević S., Ujević D., Brnada S., Šajatović B.: *Structural Multi-layered Composite Textiles Materials,* Textile Science and Economy III. Ed. Pavlović M, Zrenjanin M: University of Novi Sad., Technical faculty, 50-67 (2011)

[13] Šomođi Ž., Kovačević S., Dimitrovski K.: *Fabric Distortion After Weaving - An Approximate Theoretical Model.* 5th International Textile, Clothing and Design Conference 2010 - Magic World of Textile. Dragčević Z, Hursa Šajatović A, Vujasinović E, Eds.: p. 729-734, Dubrovnik October 2010

[14] Yilmazer U.: *Tensile, flexural and impact properties of a thermoplastic matrix reinforced by glass fiber and glass bead hybrids,* Compos. Sci. Technol., 44, 119-125 (1992)

[15] Baheti V., Militky J., Mishra R., Behera B. K.: *Thermomechanical properties of glass fabric/epoxy composites filled with fly ash*, Composites **B85,** 268-276 (2016)

[16] Petersen M. R., Chen A., Roll M., Jung S. J., Yossef M.: *Mechanical properties of fire-retardant glass fiber-reinforced polymer materials with alumina tri-hydrate filler,* Composites **B78**, 109-121 (2015)

[17] Altaweel A. M., Ranganathaiah C., Kothandaraman B., Raj J. M., Chandrashekara M.N.: *Characterization of ACS modified epoxy resin composites with fly ash and cenospheres as fillers: Mechanical and microstructural properties*, Polymer Composites **32**, 139-146 (2011)

[18] Shetty R. R., Rai S. K.: *Mechanical and Fractrographic Studies on Fly ash-filled Hydroxyl-terminated Polyurethane-toughened Epoxy Composites*, J. Compos. Materials, 43, 3231-3238 (2009)
[19] Enikolopyan N. S., Fridman M. L., Stalnova I. O. and Popov V. L.: *Filled Polymers: Mechanical Properties and Processability*, Adv. Polym. Sci., **96**, 961-967 (1990)
[20] Irfan M. S. et al.: *Lateral spreading of a fiber bundle via mechanical means*, Journal of Composite Materials ,**46**(3), 311–330 (2011)
[21] Wilson S.D.R.: *Lateral spreading of fibre tows*, J. Eng. Math., **32**, 19–26 (1997)
[22] Venkataraman M. et al.: *Sophisticated Glass Tapes for Fabrication of Composites*, Journal of Fiber Bioengineering and Informatics **12**(1) 35-42 (2019)
[23] Venkataraman M. et al.: *Stabilized Hybrid Composite Tapes for Fabrication of Composites,* Res Rept. Dept of Material Science, TUL, October 2018
[24] Jeyakumar R., Sampath P. S., Ramamoorthi R.: *Structural, morphological and mechanical behaviour of glass fibre reinforced epoxy nanoclay composites,* International Journal of Advanced Manufacturing Technology, **93**, 1-9 (2017)
[25] Barkoula N. M., Alcock B., Cabrera N. O.: *Fatigue properties of highly oriented polypropylene tapes and all-polypropylene composites*, Polymers & Polymer Composites **16**(2), 101-113 (2008)
[26] Alcock B., Cabrera N. O., Barkoula N. M., et al.: *The effect of temperature and strain rate on the mechanical properties of highly oriented polypropylene tapes and all-polypropylene composites,* Composites Science & Technology, **67**(10), 2061-2070 (2007)
[27] Thomason J. L., Vlug M. A.: *Influence of fiber length and concentration on the properties of glass fibre-reinforced polypropylene: 1. Tensile and flexural modulus,* Composites, **A27** , 477- 484 (1996)
[28] Thomason J. L.: *Micromechanical parameters from macromechanical measurements on glass rein-forced polypropylene*, Com Pos. Sci. Techn., **62,** 1455-1468 (2002)
[29] Thomason J. L.: *The influence of fiber length and concentration on the properties of glass fiber rein-forced polypropylene: 5. Injection moulded long and short fiber PP,* Composites, **A33**, 1641 - 1652 (2002)
[30] Yi P., Pengzhan Z., Jin W.: *Overview of Wind Turbine Blade Technology Development*, Journal of Hunan University of Technology, **3**(21), 48-51 (2007)
[31] Neckář B.: *Yarns*, SNTL Praha 1990 (in Czech)
[32] Higuchi K. Takai H.: *Stress–strain diagram, young's modulus, and Poisson's ratio*
of textile fibers, J. Text. Mach. Soc. Jpn., **7**, 4–12 (1961).
[33] Kittl P., Diaz G.: *Weibull's Fracture Statistics, or Probabilistic Strength of Materials, State of Art*, Res. Mechanica **24**, 99 (1988)
[34] Militký J. et. all : Proc. Int. Conf. Special Fibers, Lodz 1997
[35] Militký J: Proc. 25th. Textile Research Symposium at Mt. Fuji, August 1996

[36] Phoenix S. L., Beyerlein I. J.: *Statistical Strength Theory for Fibrous Composite Materials*, chap. 1.19 in the book A Kelly_ Carl H Zweben eds.: Comprehensive Composite Materials, Elsevier, 2000

[37] Hidalgo R. C., Kun F., and Herrmann H. J.: *Bursts in a fiber bundle model with continuous damage*, Phys. Rev. **E64**(6), 066122, (2001)

[38] Meloun M., Militký J.: *Statistical Data Analysis*, Woodhead New Delhi 2011

[39] Coleman, B. D.: *On the strength of classical fibres and fibre bundles*. Journal of the mechanics and Physics of Solids, **7**(1), 60–70. (1958)

[40] Chi Z., Chou T. W., Shen G.*: Determination of single fibre strength distribution from fibre bundle testings,* J. Mater. Sci. **19,** 3319-3324 (1984)

[41] Pan N.: *A Detailed Examination of the Translation Efficiency of Fiber Strength into Composites Strength*, Journal of Reinforced Plastics and Composites. **14**, 2-28 (1995)

[42] Harlow D. G., Phoenix L.: *The Chain-of-Bundles Probability Model for the Strength of Fibrous Materials I: Analysis and Conjectures.* J. Composite Mater.**12**, 195-214 (1978)

[43] Rinne H.: *The Weibull Distribution A Handbook*, Chapman & Hall, Boca Raton 2009

[44] Daniels H. A.: *The statistical theory of the strength of bundles of threads*, Proc. Roy. Soc. **A183**, 405 (1945)

[45] Zanakis S. H.: *A simulation study of some simple estimator for 3 parameter Weibull distribution*, J. Statist. Comput. Simul. **9**, 101-116 (1980)

[46] Marklund E., Varna J., Asp L. E.: *Stiffness and strength modelling of non-crimp fabric composites*, Collection of Technical Papers - AIAA/ASME/ASCE/AHS/ASC Structures, Structural Dynamics and Materials Conference · April 2011, pp. 1-17 (DOI: 10.2514/6.2011-1748)